Winter 12-2016

Declining Dissolved Oxygen in the Central California Current Region

Alice Ren
University of Maine, alice.ren@maine.edu

DECLINING DISSOLVED OXYGEN IN THE CENTRAL CALIFORNIA CURRENT REGION

By

Alice S. Ren

B.S. Environmental Science, Duke University, 2010

A THESIS

Submitted in Partial Fulfillment of the

Requirements for the Degree of

Master of Science

(in Oceanography)

The Graduate School

The University of Maine

December 2016

Advisory Committee:

Fei Chai, Ph.D., Professor of Oceanography, Co-Advisor

Huijie Xue, Ph.D., Professor of Oceanography, Co-Advisor

Andrew Thomas, Ph.D., Professor of Oceanography

Lawrence Mayer, Ph.D., Professor of Oceanography

Francisco Chavez, Ph.D., Senior Scientist, Monterey Bay Aquarium Research Institute (MBARI)

THESIS ACCEPTANCE STATEMENT

On behalf of the Graduate Committee for Alice S. Ren, we affirm that this manuscript is the final and accepted thesis. Signatures of all committee members are on file with the Graduate School at the University of Maine, 42 Stodder Hall, Orono, Maine.

Fei Chai, Ph.D., Professor of Oceanography (Date)

Huijie Xue, Ph.D., Professor of Oceanography (Date)

LIBRARY RIGHTS STATEMENT

In presenting this thesis in partial fulfillment of the requirements for an advanced degree at The University of Maine, I agree that the Library shall make it freely available for inspection. I further agree that permission for "fair use" copying of this thesis for scholarly purposes may be granted by the Librarian. It is understood that any copying or publication of this thesis for financial gain shall not be allowed without my written permission.

Alice S. Ren (Date)

DECLINING DISSOLVED OXYGEN IN THE CENTRAL CALIFORNIA CURRENT REGION

By Alice S. Ren

Thesis Co-Advisors: Dr. Fei Chai and Dr. Huijie Xue

An Abstract of the Thesis Presented
in Partial Fulfillment of the Requirements for the
Degree of Master of Science
(in Oceanography)
December 2016

A potential consequence of climate change is a global decrease in dissolved oxygen at depth due to changes in the balance of ventilation, mixing, respiration, and photosynthesis in the oceans. Regionally, the California Current has experienced dissolved oxygen declines since the late 1980s with observations from Oregon and the Southern California Bight. Here, we present observations of declining dissolved oxygen along CalCOFI Line 67 off of Monterey Bay, in the Central California Current region, and investigate likely mechanisms. The hydrographic cruises obtained dissolved oxygen measurements 50-300 km from shore between 1998 and 2013, with quasi-seasonal sampling resolution. Dissolved oxygen decreased along the entire transect over the 16-year period on the σ_θ 26.6-26.8 isopycnals, corresponding to depths between 250-400 m. At two regions around 130 and 240 km from shore respectively, declines in dissolved oxygen occurred on σ_θ 25.7-26.5 as well as σ_θ 26.6-26.8. Variations in oxygen concentration on isopycnals at σ_θ 25.5, at approximately the bottom of the surface mixed layer, do not show similar decline, but correlate with environmental climate indices

including the upwelling index in spring. A box model of the region suggests that multiple mechanisms are at work contributing to the oxygen declines including changes in the oxygen concentration of source waters and local respiration.

Our work highlights the need for care in investigating the mechanisms for declining dissolved oxygen in the California Current system due to the complex mechanisms at work.

DEDICATION

I dedicate this thesis to my grandparents, who inspire me and remind me that education is a privilege.

ACKNOWLEDGEMENTS

I would like to thank my primary advisor, Dr. Fei Chai, as well as my co-advisor Dr. Huijie Xue and my Univerity of Maine committee members Dr. Andrew Thomas and Dr. Lawrence Mayer for their guidance and support. I would like to thank Dr. Francisco Chavez for being a committee member, for his expertise and guidance, and for the opportunity to spend time at the Monterey Bay Aquarium Research Institute (MBARI).

I would like to thank a number of individuals at MBARI who helped me in the preliminary stages of research. They are Reiko Michisaki, Dr. Monique Messié, and Marguerite Blum of the Biological Oceanography Group and Fred Bahr of CeNCOOS. Dr. Dave Anderson was instrumental and helped to refine my skills in analysis and presentation of observational data. Countless others at MBARI made my time there enjoyable, and I thank them all.

I would like to thank all of the peers, friends, professors, teachers, staff and other generally good folks at the University of Maine and in Orono. Finally, I would like to acknowedge the following grants and programs that supported my graduate studies: the NSF IGERT graduate fellowship program, a University of Maine Graduate School Government travel grant, the David and Lucile Packard Foundation, and the MBARI Internship Program.

TABLE OF CONTENTS

LIST OF TABLES

LIST OF FIGURES

Chapter 1
INTRODUCTION

Oxygen in the world's oceans is governed by three major processes: atmospheric exchange, ocean circulation, and the balance of respiration and photosynthesis [*Wyrtki*, 1962]. Any shift in the balance of these three processes will disturb the mean dissolved oxygen concentration at a location. Indeed, among the many hypothesized impacts of climate change is widespread decrease in mid-depth dissolved oxygen in the world's ocean basins. The hypothesis suggests that increased surface heating and the resulting increased stratification of the oceans will decrease 1) the level of atmospheric exchange - less oxygen will dissolve into surface waters and 2) the mixing of surface waters to the deep ocean - less oxygen will reach deep waters [*Gruber*, 2011; *Keeling and Garcia*, 2002; *Keeling et al.*, 2010]. It is unclear whether the climate change deoxygenation hypothesis is currently producing a measureable response from the ocean [*Deutsch et al.*, 2014; *McClatchie et al.*, 2010].

Interestingly, analysis of observational ocean data from the 1980s to the 2000s has suggested a decline in dissolved oxygen in the California Current region. Reports on data off the Oregon and Washington coasts [*Chan et al.*, 2008; *Grantham et al.*, 2004; *Pierce et al.*, 2012] as well as reports from the Southern California Bight [*Bograd et al.*, 2008, 2015] suggest a decline in dissolved oxygen concentration over the roughly twenty-five-year period at a rate of 1-2 μmol/kg/year. These declines could be related to observed decreases in dissolved oxygen in the North Pacific [*Emerson et al.*, 2001, 2004; *Mecking et al.*, 2008; *Ono et al.*, 2001; *Watanabe et al.*, 2001; *Whitney et al.*, 2007] as well as in the tropical

eastern Pacific, where observations suggest an expanding oxygen minimum zone [*Stramma et al.*, 2008].

While observations have identified decreases in dissolved oxygen along the California Current region, we are far from understanding the causes of these changes. First, it is unclear whether the phenomenon is coherent across the entire California Current region. Second, it is unclear whether the changes are caused by a local increase in respiration, likely linked to changes in a physical process such as upwelling bringing extra nutrients to the euphotic zone, or from advection of water masses whose origins may be from the subarctic, the subtropical gyre, or the tropics. Third, we do not know if the observations of decreased dissolved oxygen in the California Current are part of a decadal-scale oscillation attributed to natural climate variability or triggered or exacerbated by global climate change.

In one of the earlier attempts at explanation, *Bograd et al.* [2008] suggested that changing oxygen concentrations in the Southern California Bight could be caused by local increases in stratification due to surface heating, advection of low oxygen waters from the California Current (subarctic origin), advection of low oxygen waters from the California Undercurrent (tropical origin), or advection from the Subtropical Gyre. Further, they state that they were unable to discern whether the oxygen declines had been forced locally or forced remotely and subsequently advected into the region. *Bograd et al.* [2015] suggested that advection from the California Undercurrent and from the mean subtropical gyre circulation on σ_θ 26.5 are both important contributors of low oxygen water. *Meinvielle and Johnson* [2013] focused on the California Undercurrent, using σ_θ 26.5 and bottom depths of 500-1000 m as the location of the undercurrent, and suggested that decreasing dissolved oxygen in the California Undercurrent is the cause of decreasing coastal dissolved oxygen. *Pierce et al.* [2012] studied the Newport hydrographic line and suggested that subarctic influence along σ_θ 26.6,

additional influence from the California Undercurrent on the shelf slope, and shelf processes all contribute to observed decreases in dissolved oxygen. Focusing on shelf processes and secondarily on offshore dissolved oxygen declines, *Connolly et al.* [2010] suggested that shelf respiration processes are the primary cause of shelf hypoxia in the Northern California Current.

In terms of source water changes, *Deutsch et al.* [2014] suggested that thermocline depth in the tropics drives the expansion or contraction of the volume of hypoxic waters in the tropical Pacific, with a shallower thermocline causing increased respiration and the expansion of the oxygen minimum zone. Modeled and reanalysis thermocline depths varied on the scale of 20-40 meters in the eastern tropical Pacific corresponding with periods of elevated or lower dissolved oxygen levels [*Deutsch et al.*, 2011]. Low oxygen waters from the tropics would be transported via the California Undercurrent poleward to affect the California Current region. Analysis of Station Papa at 50 °N 145 °W [*Whitney et al.*, 2007], the CLIVAR and WOCE transects at 152 °W [*Mecking et al.*, 2008], and observations in the western North Pacific [*Emerson et al.*, 2004] suggest that ventilation of σ_θ 26.6 periodically ceases, preventing replenishment of dissolved oxygen concentrations along σ_θ 26.6 throughout the subtropical gyre. *Kwon et al.* [2016] studied central mode waters in the North Pacific, defined as neutral densities of 25.6-26.6, and suggest that the area through which the oxygen-rich mixed layer is detrained into the thermocline varies decadally, with a connection to the Pacific Decadal Oscillation (PDO). The anomalously low-oxygen waters formed in the North Pacific could be transported to the California Current region in the California Current or the mean subtropical gyre circulation.

The purpose of this thesis is to present the oxygen trends and variability off of Monterey Bay, California, part of the Central California Current region, and identify and propose some mechanisms to explain observed changes. Analysis of

hydrographic dissolved oxygen data off of Monterey Bay will confirm whether dissolved oxygen levels are decreasing throughout the California Current region. Regarding mechanisms, we estimate the relative importance of different controlling factors.

Chapter 2
DATA AND METHODS

2.1 Data Collection

Cruise data were collected from 1998 to 2013 as part of various projects of the Biological Oceanography Group at the Monterey Bay Aquarium Research Institute (MBARI). Data for this analysis were from CalCOFI Line 67, at stations 67-50, 67-55, 67-60, 67-65, 67-70, 67-75, 67-80, 67-85, and 67-90 (Table 2.1). The Line 67 transect, as all CalCOFI lines, runs approximately normal to the coastline (Figure 2.1). Alongshore and cross-shore phenomena are determined with a coordinate rotation counterclockwise of 30 degrees.

Table 2.1. Line 67 hydrographic stations included in analysis

Station	Latitude (°N)	Longitude (°W)	Distance to Shore (km)	Depth (m)
67-50	36.786	-122.056	23	1006
67-55	36.620	-122.415	64	2613
67-60	36.453	-122.772	96	2954
67-65	36.286	-123.129	131	3273
67-70	36.120	-123.485	170	3581
67-75	35.953	-123.841	208	3885
67-80	35.786	-124.195	240	3964
67-85	35.620	-124.549	280	–*
67-90	35.453	-124.902	316	–*

* Data not available, but assumed to be equal to or greater than 3964 meters depth.

Dissolved oxygen data were taken with an Aanderaa optode oxygen sensor. The sensor data were averaged on 1-meter vertical depth bins. The horizontal resolution of the data was dictated by the distance between stations along Line 67, roughly 40 km. The oxygen sensor data for each cruise were calibrated with

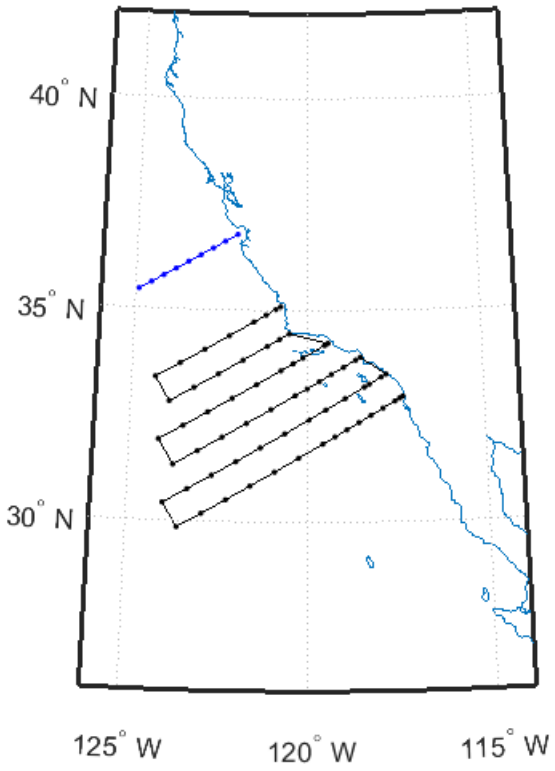

Figure 2.1. Map of the location of CalCOFI Line 67, stations 50 to 90 (blue), and the standard CalCOFI sampling lines (black).

dissolved oxygen bottle samples analyzed with a Winkler titration. Temperature and salinity observations were recorded with a CTD. Values were also averaged to 1-meter vertical depth bins.

The cruises utilized for the study were quasi-seasonal. Cruises occurred between 1 and 4 times per year, with the majority of years having more than 2 cruises.

2.2 Data Processing and Quality Control

The collection of cast data contained 714,801 sensor observations. Quality control of the data was as follows. First, data greater than 10 ml/l and at or below 0 ml/l were removed from the analysis because they were outside the normal range

of oxygen values for the region. Second, the potential density of all observations was calculated from the observed in-situ temperature and salinity, and all oxygen observations for which there were no temperature and salinity readings, or for which the temperature or salinity cast profile was deemed suspect, were removed from the analysis. In a few cases, instead of the primary temperature and salinity observations, the temperature and salinity measurements from a secondary CTD with a more realistic profile were used. Roughly 2% of the data were removed from analysis in these steps, a total of 15,586 oxygen sensor observations. Finally, all values of oxygen were calculated in μmol/kg using the molar volume of oxygen at STP of 22.3916 L/mole and the calculated potential density. One ml/L is equivalent to 44.6596 μmol/L.

2.3 Data Analysis

2.3.1 Trends on Density Surfaces

To more clearly understand ocean mixing processes and to remove the influence of heave, or isopycnal motions with no heat and salinity exchange with the environment (as defined in *Huang* [2015], although the term originates much earlier), oxygen variability was analyzed along potential density surfaces. For time-series of data along a potential density surface, there was variability due to the different stations along the transect (over 200 km long), mesoscale variability, and seasonality. We leave the mesoscale variability in the data. To look at the variability over transect stations, a chi-squared test for independence was used to determine if the oxygen values for each density were independent of the station number. To look at the variability over seasons, on each density level, and each station if variations between stations were significant, seasonal averages were computed and seasonal anomalies were used to create time-series indices. To

create time-series indices, oxygen data were binned and averaged for each day (if repeat casts were taken), then month, and then season. Months and seasons without data in the time-series were noted.

2.3.2 Climate Index Correlations

To investigate potential drivers for oxygen dynamics, oxygen time-series on specific potential densities were compared to climate indices using correlation. The chosen climate indices are important for ocean dynamics in the Pacific Ocean with variations on the timescale of 4-10 years. To represent interannual variability due to ENSO, we used the Oceanic Nino Index (ONI), which is the three-month running mean of temperature anomalies from the Nino-3.4 region (5 °S to 5 °N; 170 °W to 120 °W). To represent the North Pacific Gyre Oscillation (NPGO) we used the NPGO index downloaded from http://www.o3d.org/npgo/ and last updated on January 2016. The NPGO is the second mode of sea surface height variability in the North Pacific which is related to the strength of the subtropical gyre circulation [*Di Lorenzo et al.*, 2008]. To represent local upwelling, we used the NOAA PFEL upwelling index for the period 1998-2013 at 36 °N 122 °W. The index is calculated from the geostrophic wind stress which is derived from sea level pressure from the U.S. Navy Fleet Numerical Meteorology and Oceanography Center's operational forecasts. We used the monthly mean anomalies downloaded from http://www.pfeg.noaa.gov/products/PFELData/ upwell/monthly/upanoms.mon. In addition, we used the multivariate ocean climate index (MOCI) developed for the Farallon Islands and north-central California. The index incorporates basin scale indices related to El Nino Southern Oscillation including the ONI, Southern Oscillation Index (SOI), and multivariate ENSO index (MEI); subarctic indices including the North Pacific Index (NPI), NPGO, and Pacific Decadal Oscillation (PDO); as well as upwelling indices, wind

stress, sea level, sea surface temperature, salinity, air temperature, and precipitation [*Sydeman et al.*, 2014]. The MOCI is a representation of local oceanic climate. Positive index values represent subtropical, warm, rainy years with weak winds and weak upwelling while negative index values represent years with strong subarctic influence, cold sea surface temperatures, strong winds and upwelling. Sea surface temperature, sea level, precipitation, air temperature and other variables used in MOCI were taken from observations in the Central California region; thus, MOCI should be a good index of climate variability for Line 67.

To compare climate index and dissolved oxygen variability, variation in indices and oxygen time-series were normalized by standard deviations and compared on a seasonal basis. Seasonal time-series were defined with winter as December through February, spring as March through May, summer as June through August, and fall as September through November except in comparisons to the MOCI. The MOCI is a seasonal index defined by winter as January to March, spring as April to June, summer as July to September, and fall as October to December. The seasonal dissolved oxygen time-series was defined with MOCI seasonal definitions in the MOCI comparison.

A major complication in correlation of geophysical and climate phenomena is autocorrelation of time-series data [*Bartlett*, 1935; *Wunsch*, 1999]. Consequently, all correlations were tested for lag-1 autocorrelation. If significant autocorrelation were detected, the true significance of the correlation was corrected by using an effective sample size when calculating the t-statistic and as the sample size to calculate the p-value [*Santer et al.*, 2000]. The effective sample size, n_e, is defined according to the lag-1 autocorrelation coefficient r_1 and the original sample size n by:

$$n_e = n\frac{1 - r_1}{1 + r_1}.$$

If the correlation were still significant after using n_e, the correlation (R-value) was corrected using the lag-1 autocorrelation coefficient and the Cochrane-Orcutt procedure [*Cochrane and Orcutt*, 1949].

2.3.3 Regression Models

To investigate spatial patterns of oxygen dynamics, changes in time of oxygen concentration were assessed at each isopycnal and station. Observations were binned to 0.1 σ_θ and by station. Station 50 was removed from the analysis due to low number of observations. Statistics were performed on anomalies from the seasonal means of the observations during 1998-2013. Data were averaged temporally by day (if repeat casts were taken for a station).

The correlation (R-value), significance of the correlation (p), and the constants for a linear model (mx+b, where time was the x-variable) were calculated for each 0.1 σ_θ and station bin. To map the calculations back to coordinates for depth and distance offshore, statistics along isopycnals were taken to represent changes on the average depth of each isopycnal in the analysis.

2.3.4 Alongshore Velocity

In-situ temperature and salinity were used to calculate alongshore geostrophic velocities. Temperature and salinity observations were binned to 5-meter depth intervals and by station. Seasonal averages were calculated, with winter defined as December-February, spring defined as March-May, summer defined as June-August, and fall defined as September-November. Geostrophic velocities were calculated with a reference depth of 800 meters. The reference depth was chosen as a compromise between depth and the availability of temperature and salinity observations. It is possible that there exists a level of motion at 800 meters depth, in which case the geostrophic velocities presented are actually the shear relative to

800 meters. However, relative patterns and the interpretation given here remain valid. Additional data from ADCP instruments or other methods which measure the velocity could calibrate the velocities presented here.

Chapter 3
RESULTS

The climatological seasonal (Figure 3.1) and mean (Figure 3.2) dissolved oxygen level along Line 67 from 1998-2013 demonstrate that off of Monterey Bay the surface layer is well oxygenated while waters become hypoxic (defined as 60 μmol/kg) at around 300-350 meters depth. Seasonally, there are changes in the depth of an oxygen concentration surface. The tilting of isopycnals in spring causes corresponding oxygen surfaces to tilt upwards in the upper 150 m. Below 150 m, the oxygen along an isopycnal is lower closer to shore and increases offshore. The

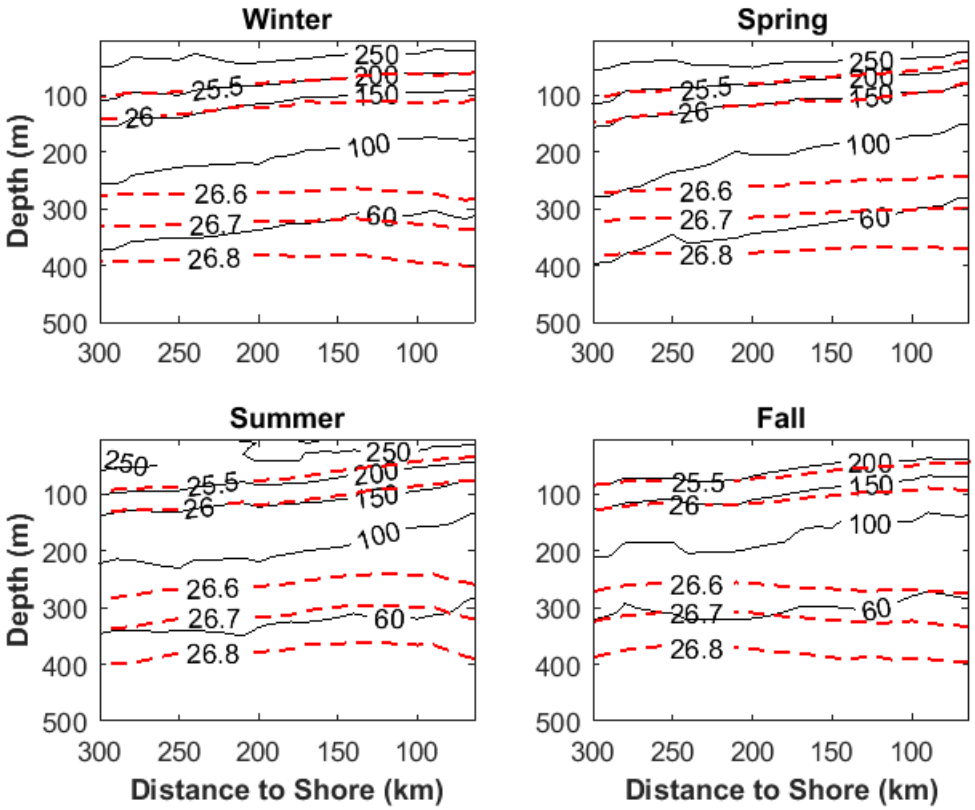

Figure 3.1. Seasonal dissolved oxygen (black, solid) along Line 67 (μmol/kg). The contours of potential densities 25.5, 26.0, 26.6, 26.7, and 26.8 are drawn (red, dashed).

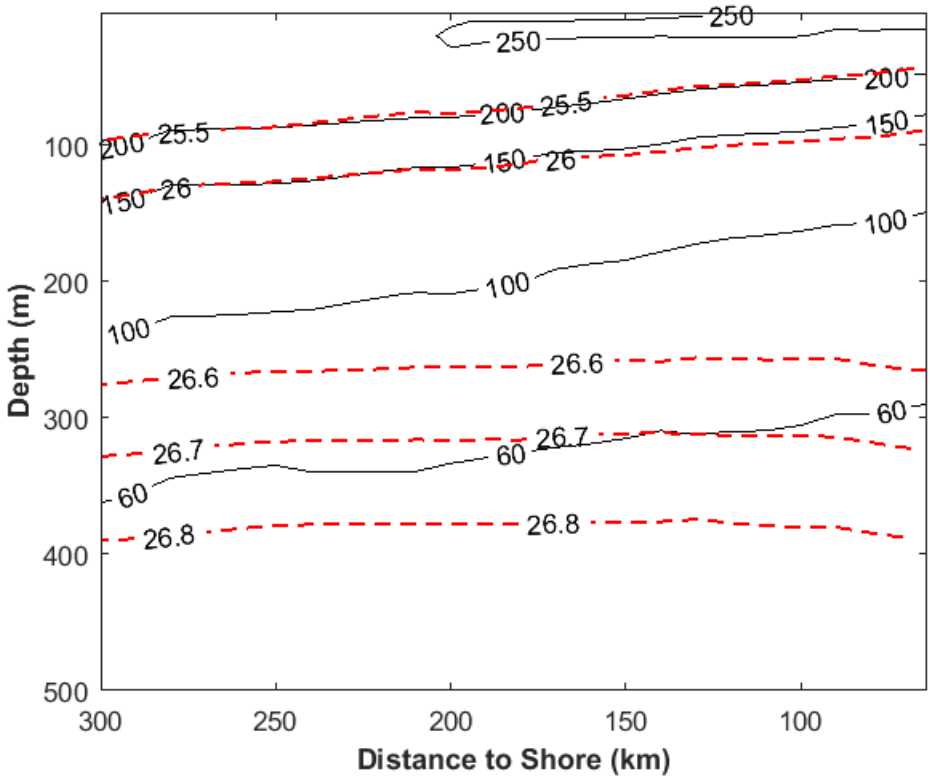

Figure 3.2. Mean dissolved oxygen along Line 67 (μmol/kg). The contours of potential densities 25.5, 26.0, 26.6, 26.7, and 26.8 are drawn (red, dashed).

density surfaces for σ_θ 26.6-26.8 characteristically tilt downward close to shore, indicating the location of poleward alongshore flow of the California Undercurrent.

The climatological alongshore velocity along Line 67 (Figure 3.3) demonstrates the poleward California Undercurrent as well as the equatorward California Current in the upper 200 m. The hydrographic data from station 50, 23 km offshore in Monterey Bay, were few, so station 50 was not included in the alongshore velocity calculation. Thus, the core of the California Undercurrent appears inshore of the plotted alongshore velocities. Below 250 m and from 125-300 km to shore is a region of very low mean alongshore current speed. Within the interior region of low mean current speed, the demarcation between poleward and equatorward flow is around 210 km. The demarcation is closer to shore at

shallower depths, roughly 130 km from shore at 200 m depth and within 100 km at the surface.

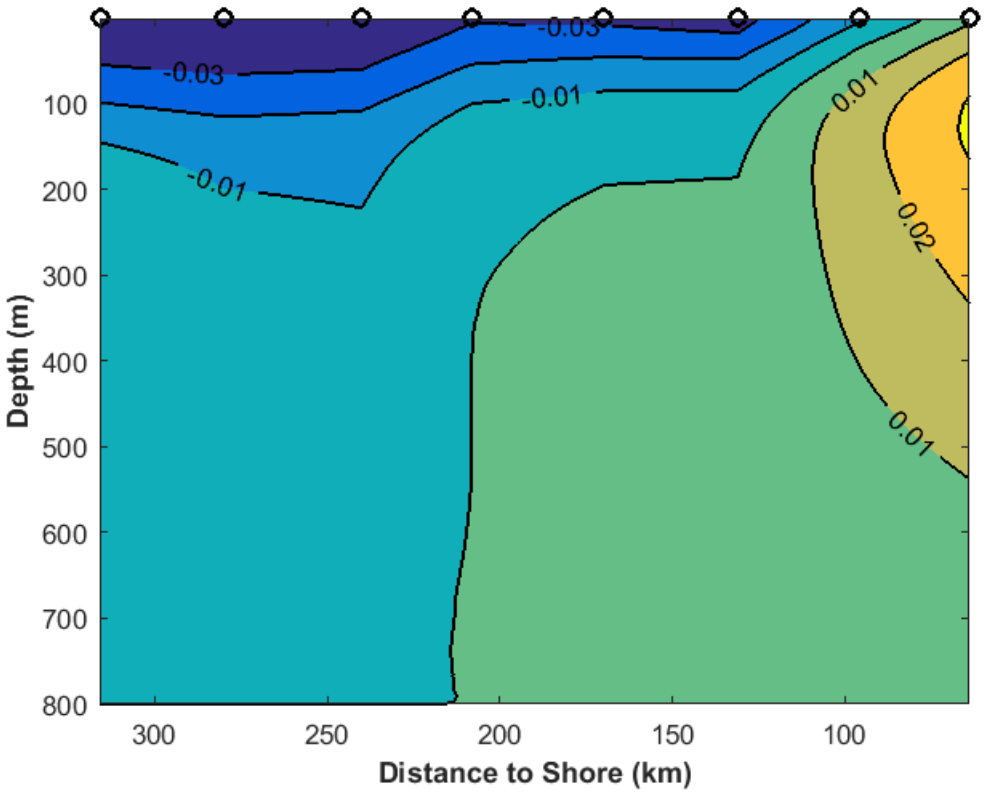

Figure 3.3. Average alongshore velocity along Line 67 (m/s). Positive values denote poleward alongshore flow. Black circles mark hydrographic stations.

3.1 Oxygen Dynamics with Density and Depth

Analysis of changes in oxygen concentrations were examined on isopycnals to eliminate the influence of heave and because most of the mixing of dissolved oxygen should occur by isopycnal mixing. However, there are interesting differences in the oxygen dynamics of isopycnals with depth (Figure 3.4). On σ_θ 25.5, found at roughly 50-100 m depth, the dissolved oxygen concentrations have stronger interannual variability and potentially exhibit a low-frequency oscillatory pattern with a period of less than 10 years. On σ_θ 26.7, found at roughly 300-350

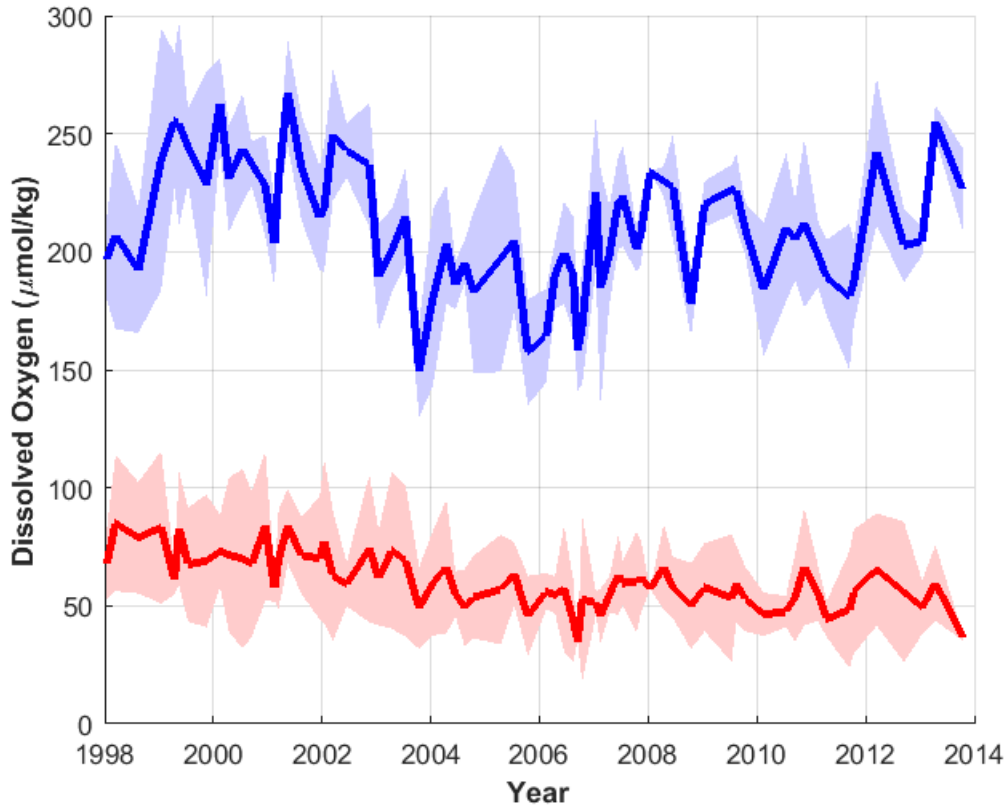

Figure 3.4. Line 67 dissolved oxygen concentrations along σ_θ 25.5 (blue) and σ_θ 26.7 (red) from 1998 to 2013. Shaded error bars represent two standard deviations from the mean.

m depth, the interannual variability is smaller, and over 1998-2013 there appears to be a linear decline in dissolved oxygen. While at σ_θ 26.7 the stations closer to shore had lower dissolved oxygen, a similar trend was found in all stations, justifying the presentation of the dynamics of σ_θ 26.7 as the average over all the stations of the transect. On σ_θ 25.5, there was no significant difference in the dissolved oxygen concentration among stations.

The low frequency inter-annual signal from σ_θ 25.5 disappears at σ_θ 26.6, at roughly 280 m depth, where a decreasing linear trend in dissolved oxygen with time emerges. The linear declining trend disappears again at σ_θ 26.9, at roughly 470 m depth, beneath which there appears to be no, or very little, temporal trend

in the oxygen concentration. From σ_θ 26.9-27.5, there is no, or very little, temporal trend in dissolved oxygen. Data availability for dissolved oxygen data is low below 800 m or around σ_θ 27.2. Though casts were occasionally taken to 1000 m and deeper, such deep casts were not taken with sufficiently high frequency to investigate a temporal trend.

3.2 Upper Level Oxygen Variability

Time-series indices of oxygen anomalies along σ_θ 25.5 were correlated against the ONI, NPGO, upwelling and MOCI climate indices to investigate possible climate drivers of year-to-year variability.

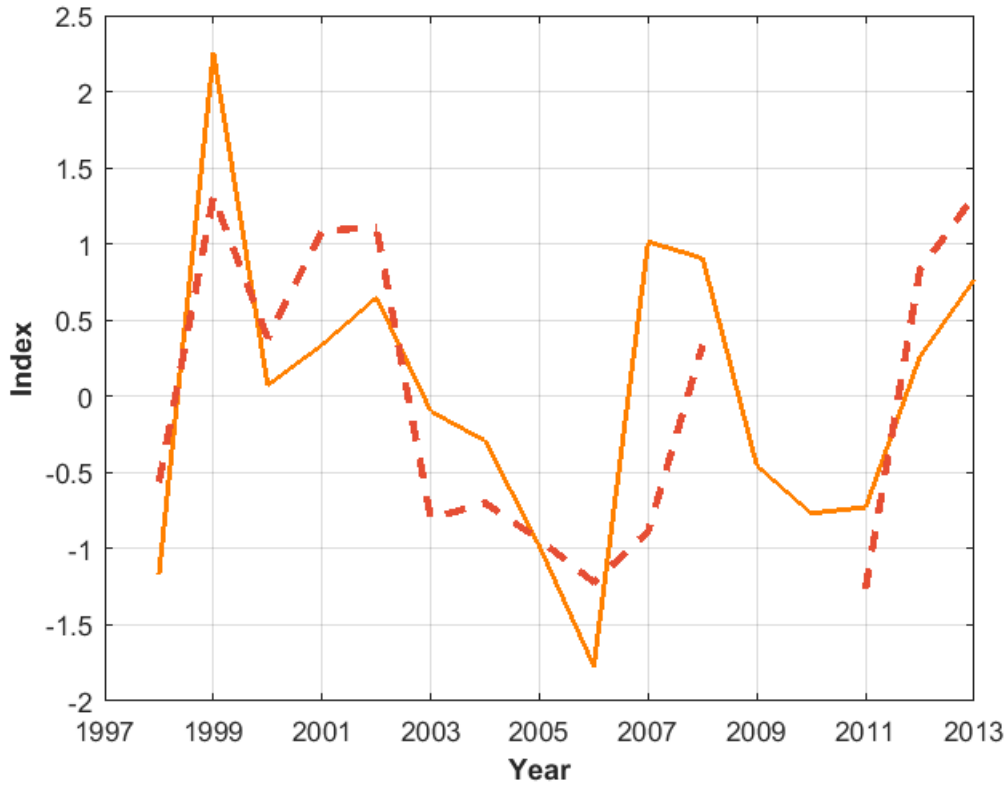

Figure 3.5. Spring upwelling index (orange, solid) and the spring dissolved oxygen index of anomalies on σ_θ 25.5 (red, dashed) from 1998-2011. Dissolved oxygen data were not available for spring 2009 and 2010.

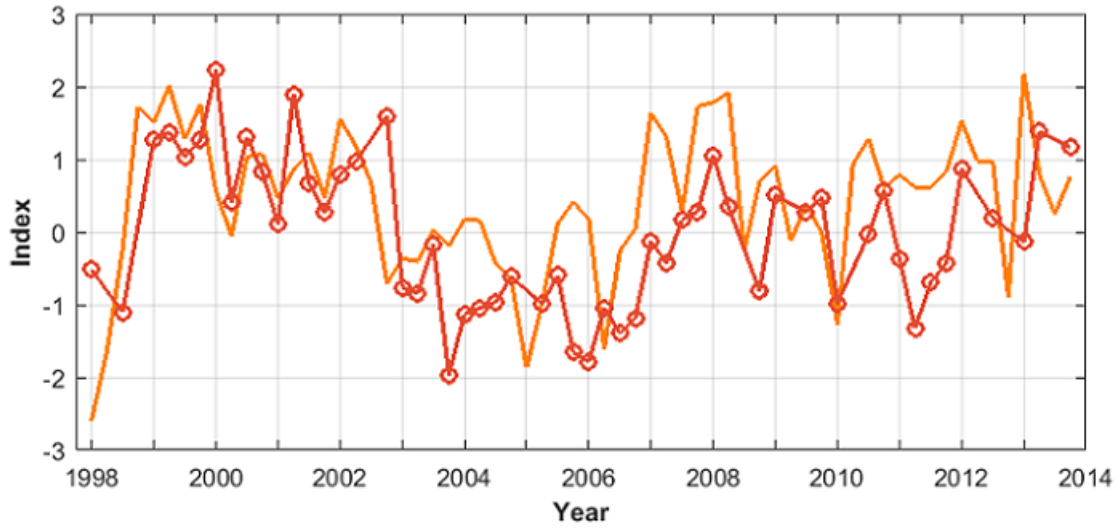

Figure 3.6. MOCI index (orange, solid) and the seasonal dissolved oxygen index of anomalies on σ_θ 25.5 (red, circles) from 1998-2013. Seasons are defined as January-March, April-June, July-September, and October-December in accordance with the MOCI index.

After correcting for autocorrelation, correlations were not significant to the 99% confidence level with the El Nino ONI index ($p < 0.30$) and the NPGO ($p < 0.02$). The confidence level was relaxed to 98%, at which the NPGO would be significant; however, there was lag-1 autocorrelation with the oxygen time series and the NPGO. The correlation was corrected using the Cochrane-Orcutt procedure. The resulting correlation for the corrected indices was very low ($R = -0.13$, $p = 0.31$) suggesting that the majority of the linear fit between the NPGO and dissolved oxygen was due to autocorrelation.

The monthly dissolved oxygen relationship with the monthly upwelling index was not significant ($p = 0.047$, no significant autocorrelation). However, comparing only the spring (Mar-May) average for the upwelling index and the dissolved oxygen index, the correlation was high and significant ($R = 0.71$, $p < 0.01$, no significant autocorrelation). The indices show good agreement visually (Figure 3.5) though the time series is relatively short (n=14). The importance of

spring may be due to the onset of upwelling earlier or later in the year as well as the strength of upwelling in the spring months.

The MOCI was weakly correlated with the dissolved oxygen index (-0.36, $p < 0.01$) after correcting for autocorrelation using the Cochrane-Orcutt procedure. In contrast to the upwelling index's importance in spring, the relationship is year-round. The MOCI relationship appears very strong in the early 2000s but weakens towards the end of the time series (Figure 3.6). The differences between the MOCI and the upwelling index are the additional indices included in MOCI which compensate for the mismatch in seasons other than spring. However, various factors including the behavior of the additional climate indices differing from that of the upwelling index lead to a weaker correlation.

3.3 Mid-Depth Decreases in Dissolved Oxygen

Decreases in dissolved oxygen occurred on σ_θ 26.6-26.8 for almost all stations (Figure 3.7) and ranged from -0.57 to -2.73 μmol/kg/year. For stations 65, 75, and 80 linear declines in dissolved oxygen were also found between σ_θ 25.5-26.6. Very strong linear declines (-2.35 to -2.71 μmol/kg/year) were found between σ_θ 25.7 and 26.5 on station 80, roughly 240 km from shore.

Mapped from density to depth coordinates (Figure 3.8), there is a strong area of declining dissolved oxygen from 200-250 km from shore at 100-250 m, around 130 km from shore at 100-250 m, and through the entire transect at depths of 250-400 m.

The declines along σ_θ 26.7 represent declines of areas at the hypoxic boundary (60 μmol/kg). In 1998, the average station oxygen concentration at σ_θ 26.7 was 76.9 μmol/kg. The average rate of decline of dissolved oxygen along σ_θ 26.7 was 1.92 μmol/kg/year. Thus, the average station oxygen concentration at the end of

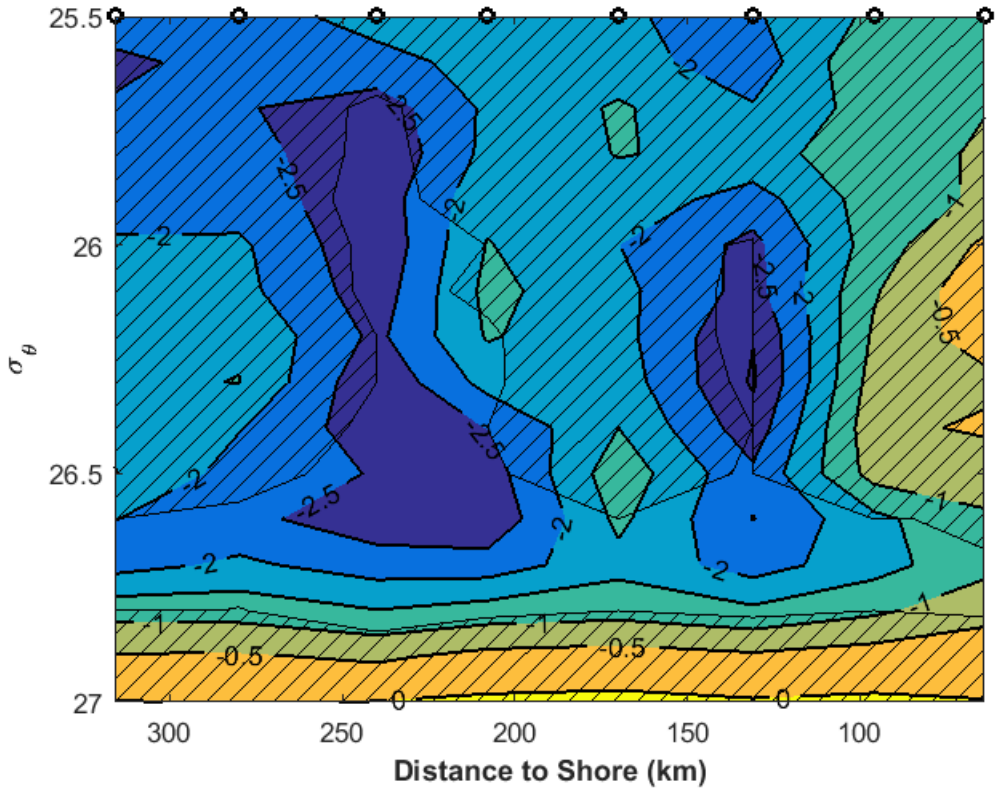

Figure 3.7. Rate of change in dissolved oxygen concentration over time (μmol/kg/year) from 1998 -2013 on σ_θ 25.5-27.0. Hatched areas represent where the rate of decline was not statistically significant (p>0.01). Black circles mark hydrographic stations.

2013 according to the linear model was 46.2 μmol/kg. Along σ_θ 26.7 the average percentage loss in dissolved oxygen concentration was 39.9 percent during 1998-2013.

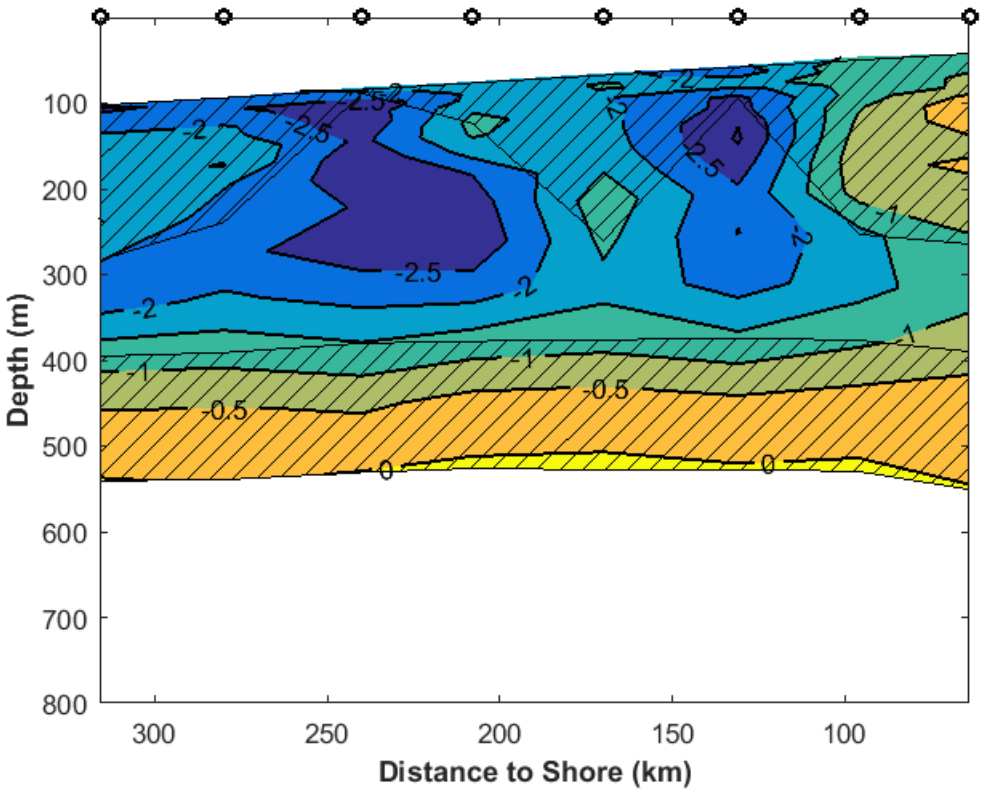

Figure 3.8. Rate of change in dissolved oxygen concentration over time (μmol/kg/year) from 1998-2013 on depth. The rate of change was calculated along isopycnals and is plotted over the average depth of each σ_θ from 25.5-27.0. Hatched areas represent where the rate of decline was not statistically significant ($p>0.01$). Black circles mark hydrographic stations.

Chapter 4
DISCUSSION

4.1 Coherence of Declines

The results of Line 67 off of Monterey Bay suggest that there is significant decline in dissolved oxygen occurring in the northern, central and southern California Current regions, which suggests that the deoxygenation phenomenon is coherent across the California Current system. South of Line 67 in the Southern California Bight, *Bograd et al.* [2015] found declines on σ_θ 26.5 of 1-2 μmol/kg/year. North of Line 67, along the Newport, OR hydrographic line at 44.66 °N, *Pierce et al.* [2012] found declines up to 0.9 μmol/kg/year on σ_θ 26.3-26.5. Declines in the North Pacific including Ocean Station Papa have been at the rate of about 0.5-1 μmol/kg/year (Table 4.1).

Table 4.1. Summary and comparison of rates of decline in the California Current and Northeast Pacific.

Researcher	Density	Decline (μmol/kg/yr)	Time Period	Region
Bograd et al. 2015	26.5	-1 to -2	1984-2012	S. California Bight
Pierce et al. 2012	26.3-26.5	-0.3 to -0.9	1960s-2000s	Newport, Oregon Line
Mecking et al. 2008	26.6	-0.5 to -1.1	1994-2004	152 °W
Whitney et al. 2007	26.3-27.0	-0.4 to -0.7	1950s-2006	Ocean Station Papa (50 °N, 145 °W)
This Study	26.7	-1.92	1998-2013	Line 67, Central California

The California Current dissolved oxygen declines are of similar magnitude to the North Pacific observations [*Mecking et al.*, 2008; *Whitney et al.*, 2007] which have

suggested a basin-wide mid-depth decline in dissolved oxygen. The rate of decline along the southern and central California coasts is larger, and thus it is possible that the driving process in the region is more extreme and/or incorporates other processes. Differences in frequency of observations (for example, *Mecking et al.* [2008] calculated the difference between only two points in time) and other sampling issues could also factor into the difference.

4.2 On the Nature of Oxygen Variability

Assessing dissolved oxygen dynamics on isopycnals rather than at the measured depth is important because it removes the effects of heave, minimizing variability due to internal waves and seasonal adjustments of isopycnals. Secondarily, there may be interannual variation in the depth of isopycnals. In this study, it is suggested that σ_θ 25.5 shoals during years with strong spring upwelling. The density surfaces 25.5 and 26.7 lacked significant long-term trends of changes in depth, in either inshore stations (stations 55-65) or offshore stations (stations 75-85) during the time period.

The hypothesized reason for the differences in decadal variability in σ_θ 25.5 and σ_θ 26.7 is the influence of the winds. Higher upwelling generates increased concentrations of dissolved oxygen on σ_θ 25.5 because upwelling raises the isopycnal higher in the water column, exposing it to more oxygenated waters. There may also be an effect of stronger primary productivity during a year with stronger spring upwelling, part of which could be due to a longer upwelling season from an earlier start. The Ekman depth or the original depth of upwelled waters is thought to be no deeper than 200 meters in the Central Californa region [*Chhak and Di Lorenzo*, 2007]. Thus, while σ_θ 25.5 is affected by interannual variability of the wind stress, σ_θ 26.7 is not.

In the Central California upwelling region, the influence of upwelling in the spring appears to set the stage for the oxygen variability for the entire year (Figure 4.1). The upwelling index during the summer, fall, and winter has an inter-annual pattern that differs from that of spring. On the other hand, the inter-annual pattern for oxygen is similar for all seasons, with slight differences in magnitude. It is possible that the spring upwelling season is the dominant dynamical event for the year which oxygenates the surface layers to a greater or lesser degree from one year to the next.

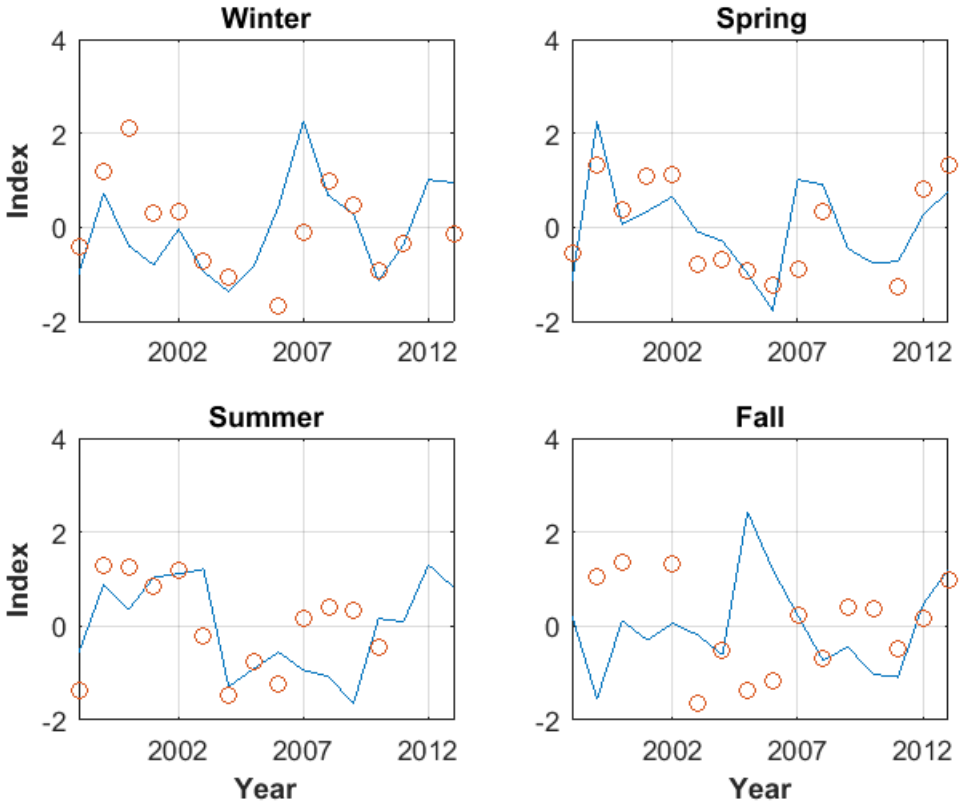

Figure 4.1. Seasonal anomalies of dissolved oxygen (circles, orange) and seasonal upwelling index anomalies (solid line, blue). Anomalies were normalized by the seasonal standard deviation to create index values. Seasons are defined with December-February as winter, March-May as spring, June-August as summer, and September-November as fall.

Further, the difference in variability of dissolved oxygen on an isopycnal at 50-100 m, a part of or at the bottom of the mixed layer, and an isopycnal at 300-350 m is significant in terms of the ability to detect trends. For σ_θ 25.5, the year-to-year variability in oxygen is strong enough to mask a clear long-term trend for the time period. In other words, natural variability or decadal variability is significant in the surface layer isopycnals.

Natural variability has implications for the study of properties on isopycnals found in or near the mixed layer. *Bograd et al.* [2015] used the isopycnal σ_θ 25.8 to signify the California Current, and they found no statistically significant trend in dissolved oxygen concentration on the isopycnal. Large inter-annual variations in oxygen may be the dynamics most noteworthy on mixed layer isopycnals. The results from *Bograd et al.* [2015] are in agreement with the results here from Central California, where we also see no long-term trend on isopycnal σ_θ 25.8 except at station 80.

4.3 Processes Causing Declining Dissolved Oxygen

From the observations along Line 67, we can attempt to better understand why the dissolved oxygen in Central California has declined. Previous studies suggest that there may be more than one process at work. To that end, we use a box model to estimate major processes acting in concert. The goal is to reproduce the declines in the observational results presented here with a reasonable set of environmental forcings.

4.3.1 Model Formulation

There are multiple potential causes of, or contributors to, the oxygen declines along Line 67. The mechanisms of dissolved oxygen decline can be divided into a) local causes increasing the local respiration, likely linked to increased primary

production and particulate organic carbon (POC) flux, b) remote forcing through changes in source water concentration or volume transport of the alongshore currents (California Current or California Undercurrent), or c) remote forcing through a North Pacific Subtropical Gyre phenomenon at depth spreading through isopycnal mixing. While large-scale ocean models have suggested the importance of stratification, we find very little long-term movement in isopyncal depths over time in our observations. Thus, we do not include stratification effects in our box model.

In the box model, we include the local respiration and the alongshore currents and their source waters. From the mean alongshore velocity (Figure 3.3), there is a division between mean poleward flow and mean equatorward flow that, at σ_θ 26.7, occurs around 210 km from shore. The division of nearshore waters into a mean poleward regime and equatorward regime is supported by other observational studies [*Chelton*, 1982; *Hayward and Venrick*, 1998; *Collins et al.*, 2003]. The demarcation between calculated mean poleward flow and mean equatorward flow occurs around 100 km at the surface and 150 km at 200 m, which agrees with *Collins et al.* [2003]. At around 300 m, where a linear decline in oxygen was observed, the demarcation is around 200 km from shore, which appears reasonable but cannot be compared to *Collins et al.* [2003] who only calculated the velocities at the surface and 200 m. As suggested by the low mean alongshore current speeds, the region below 100 m and at least 100 km from shore is dominated by meandering currents and eddy activity.

It is curious that the decline in dissolved oxygen occurs in both the region of mean poleward flow and mean equatorward flow. It also appears that the two regions of high rate of oxygen decline that are shallower than σ_θ 26.7 exist in the regions of mean poleward flow and mean equatorward flow, while in the area where the alongshore velocity switches sign, the rate of change is not statistically significant or low (Figure 3.8). Though there are seasonal shifts in the separation

between the mean poleward and mean equatorward currents, the shifts are only around 25 km in magnitude [*Collins et al.*, 2003]. Thus, it is important to include poleward and equatorward alongshore flow in the box model. Because it is difficult to estimate the spreading of low oxygen water due to a subtropical gyre phenomenon, we do not include it in the model explicitly though it can be considered as affecting the northern source water. In the box model, we can answer the question of whether changes in the alongshore flow, current source waters, or local respiration could have caused the observed decrease in dissolved oxygen along σ_θ 26.7.

The model is set up with two boxes. One represents the inshore, mean poleward flow. The other represents the offshore, mean equatorward flow. The boxes represent the interior of the ocean at around 300 m depth. The boxes are 100 m in height, 50 km in the cross-shore direction, and 78.8 km in the alongshore direction. The mean alongshore velocity is chosen to be 0.01 m/s towards the equator in the offshore box and 0.01 m/s towards the pole in the inshore box. The timestep of the model is taken to be a quarter of a year to represent a seasonal timescale. In a quarter of a year, a particle traveling 0.01 m/s journeys 78.8 km, thus the choice of length for the alongshore size of the box.

The source water concentration of dissolved oxygen from the North and South are chosen using the World Ocean Atlas. The World Ocean Atlas is calculated on a 1°x1° grid. The northern source water is chosen from 39.5 °N, 127.5 °W. The southern source water is chosen from 31.5 °N, 117.5 °W. The northern source water is 505 km distance from station 80 on Line 67. The southern source water is 743 km distance from station 65 on Line 67. The southern source water is off Baja California and was chosen to be farther from the region to avoid sampling near the complex circulation of the Southern California Bight.

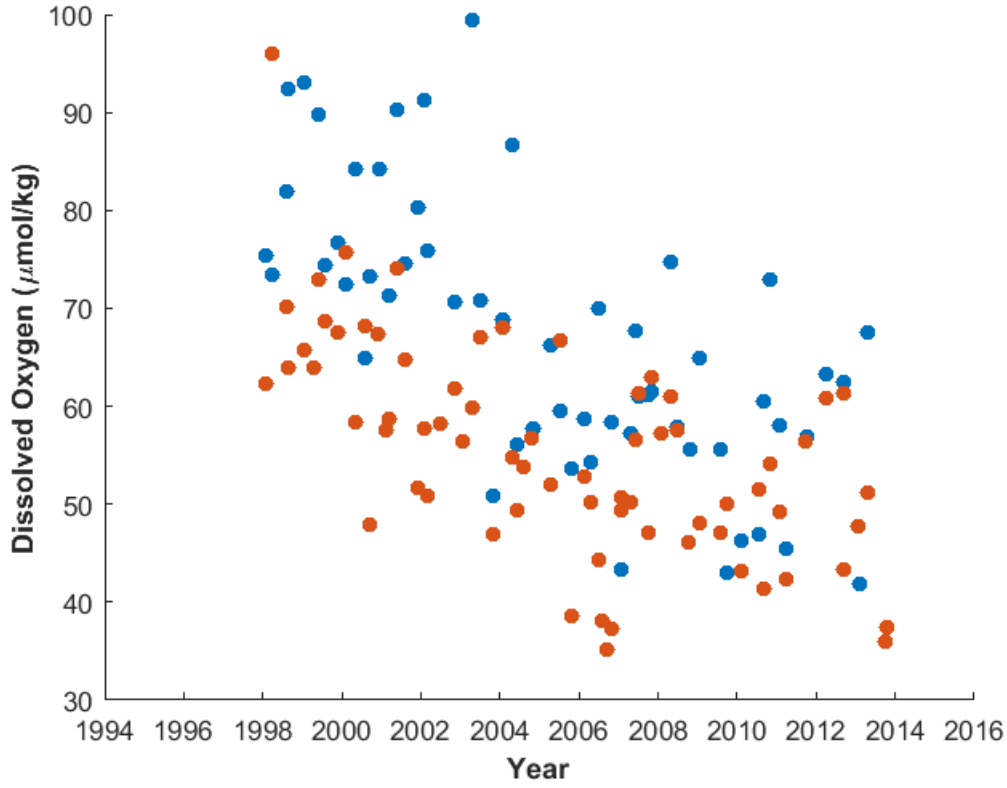

Figure 4.2. Inshore (average of stations 55-65, orange) and offshore (average of stations 75-85, blue) dissolved oxygen over time along σ_θ 26.7.

The concentrations of dissolved oxygen in the inshore and offshore boxes at the start of the model run are taken from the average inshore (stations 55-65) and offshore (stations 75-85) station oxygen concentrations in roughly 1999 (Figure 4.2). The cross-shore gradient in oxygen is an important feature on σ_θ 26.7. The cross-shore oxygen gradient was maintained in the observations even as dissolved oxygen declined along the entire transect. (Note that in Figure 3.4 the average dissolved oxygen across the transect was plotted which masked the cross-shore gradient.) The starting dissolved oxygen concentrations for the offshore box and the inshore box were chosen to be 80 and 71 μmol/kg respectively based on the finding that linear regression models of station 80 and station 65 were roughly 9 μmol/kg different at the start of the time period.

The fluxes of oxygen into the onshore and offshore boxes are calculated with the mean flow and the concentration gradient between the source waters and the box oxygen concentrations. The unknowns that remain for the two boxes are the respiration, the only biological component since at 300 m depth we assume no photosynthesis, and the cross-shore mixing between the inshore and offshore box. If we assume that the respiration in each of the boxes is the same, which is a reasonable assumption for 300 m depth, then we have two equations and two unknowns; thus we can solve for the steady state respiration and the steady state cross-shore mixing.

We parameterize the cross-shore mixing using a Fick's law formulation, with a mixing parameter D. From the steady state cross-shore mixing, we can find D because we know the steady state cross-shore oxygen gradient.

The model is represented in the schematic Figure 4.3. At steady state, the annual net flux of oxygen into the offshore box is 12.5 μmol/kg and the annual net oxygen deficit in the inshore box is 9.13 μmol/kg. Between this difference, 10.8 μmol/kg per year is mixed in the cross-shore direction. In both the inshore and offshore boxes the annual respiration rate is 1.68 μmol/kg. The equilibrium respiration is reasonable looking at the estimated respiration from Martin curves at around 300 m [*Martin et al.*, 1987]. The value of D is 209.5 m^2/s which, if a mean eddy speed is 0.01 m/s, suggests a mean eddy length scale of 21 km. A survey of eddy characteristics of the region as obtained from RAFOS floats suggests that 0.01 m/s and an eddy length scale of 30 km is reasonable [*Garfield et al.*, 1999, 2001; *Collins et al.*, 2004, 2013], suggesting that the calculated D is reasonable. Thus, we have confidence that the model is a reasonable representation of the system at steady state.

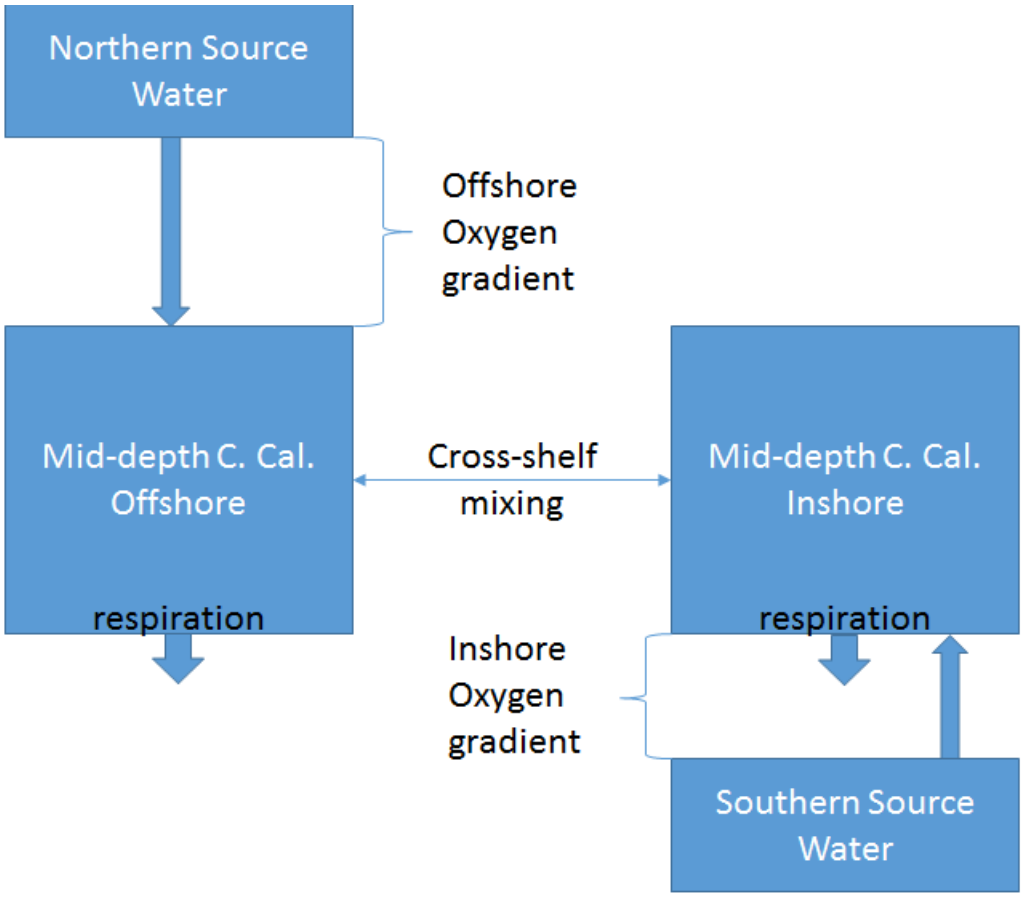

Figure 4.3. Schematic diagram of box model

4.3.2 Perturbations and Model Runs

We tested three sets of perturbations to the system: 1) declines in the source water dissolved oxygen concentrations 2) changes in the mean alongshore velocity and 3) changes in local respiration. For the perturbations, we also tested whether there was a one-time switch to a new state, or whether the perturbation needed to continue and in effect grow over time. We also considered multiple perturbations acting at the same time.

The model runs are summarized in table 4.2. Responses are the total change in dissolved oxygen concentration for inshore and offshore boxes for the model simulation time period, 20 years.

Table 4.2. Summary of Box Model Runs

Perturbation	Response: Inshore (μmol/kg)	Response: Offshore (μmol/kg)
Source Water: Step Function		
Southern 5 μmol/kg	-2.6	-1.7
Northern 5 μmol/kg	-2.5	-3.4
Both 5 μmol/kg	-5.1	-5.1
Southern 15 μmol/kg	-7.8	-5.1
Northern 15 μmol/kg	-7.5	-10.3
Both 15 μmol/kg	-15.4	-15.4
Source Water: Continuous		
Southern 1 μmol/kg/year	-9.5	-6.1
Northern 1 μmol/kg/year	-9.0	-12.5
Both 1 μmol/kg/year	-18.5	-18.6
Southern 2 μmol/kg/year	-19.1	-12.2
Northern 2 μmol/kg/year	-17.9	-25.0
Both 2 μmol/kg/year	-37.0	-37.3
Southern 3 μmol/kg/year	-28.6	-18.3
Northern at 1 and Southern at 2 μmol/kg/year	-28.0	-24.7
Alongshore Velocity: Continuous		
Offshore 1 cm/s to 0.5 cm/s	-6.1	-8.6
Inshore 1 cm/s to 2 cm/s	-7.1	-4.6
Inshore to 0.5 cm/s and Offshore to 2 cm/s	-12.1	-13.3
Inshore to 0.5 cm/s and Offshore to 3 cm/s	-14.9	-15.6
Respiration: Continuous		
Inshore 1.68-2.68 μmol/kg/year	-4.5	-2.9
Offshore 1.68-2.68 μmol/kg/year	-2.9	-4.0
Both 1.68-2.68 μmol/kg/year	-7.4	-6.9
Inshore 1.68-3.68 μmol/kg/year	-9.0	-5.7
Offshore 1.68-3.68 μmol/kg/year	-5.7	-8.0
Both 1.68-3.68 μmol/kg/year	-14.7	-13.8
Cross-shore Mixing, D: Continuous		
Increase 8 m^2/s per year	2.1	-1.5
Decrease 8 m^2/s per year	-8.1	6.0
Multiple Factor		
Northern at 1 and Southern at 2 and 50% Respiration Increase	-34.2	-30.5

4.3.2.1 Perturbations in Source Water Oxygen Concentration

The source water declines were tested for a one time change in the source water concentration, or a step function perturbation. The source water oxygen concentration at the start of the simulation changed from the steady state concentration to a new (lower) dissolved oxygen concentration. A mechanism for a step function perturbation in the source water would be a sudden change from a more oxygenated to a less oxygenated ocean state in the source water region. Changes of 5 and 15 μmol/kg were tested for the northern source water only, the southern source water only, and in both sourcewaters (Figure 4.4).

Immediately, it is apparent that a stepfunction perturbation was not able to explain a continuous decline over 15-20 years. The system reached a new equilibrium concentration for the inshore and offshore boxes in around 6 years. Further, a 15 μmol/kg decline in source waters of both the north and south was necessary to reproduce a magnitude of decline approaching the observed declines which, at 1.9 μmol/kg/year, would have been 38 μmol/kg over 20 years. When only one source water decreased, the inshore and offshore boxes shared the effect, with the oxygen concentrations in each box decreasing less than the source water decrease. The model demonstrated the effect of cross-shore mixing and dissipation of the perturbation in the alongshore direction.

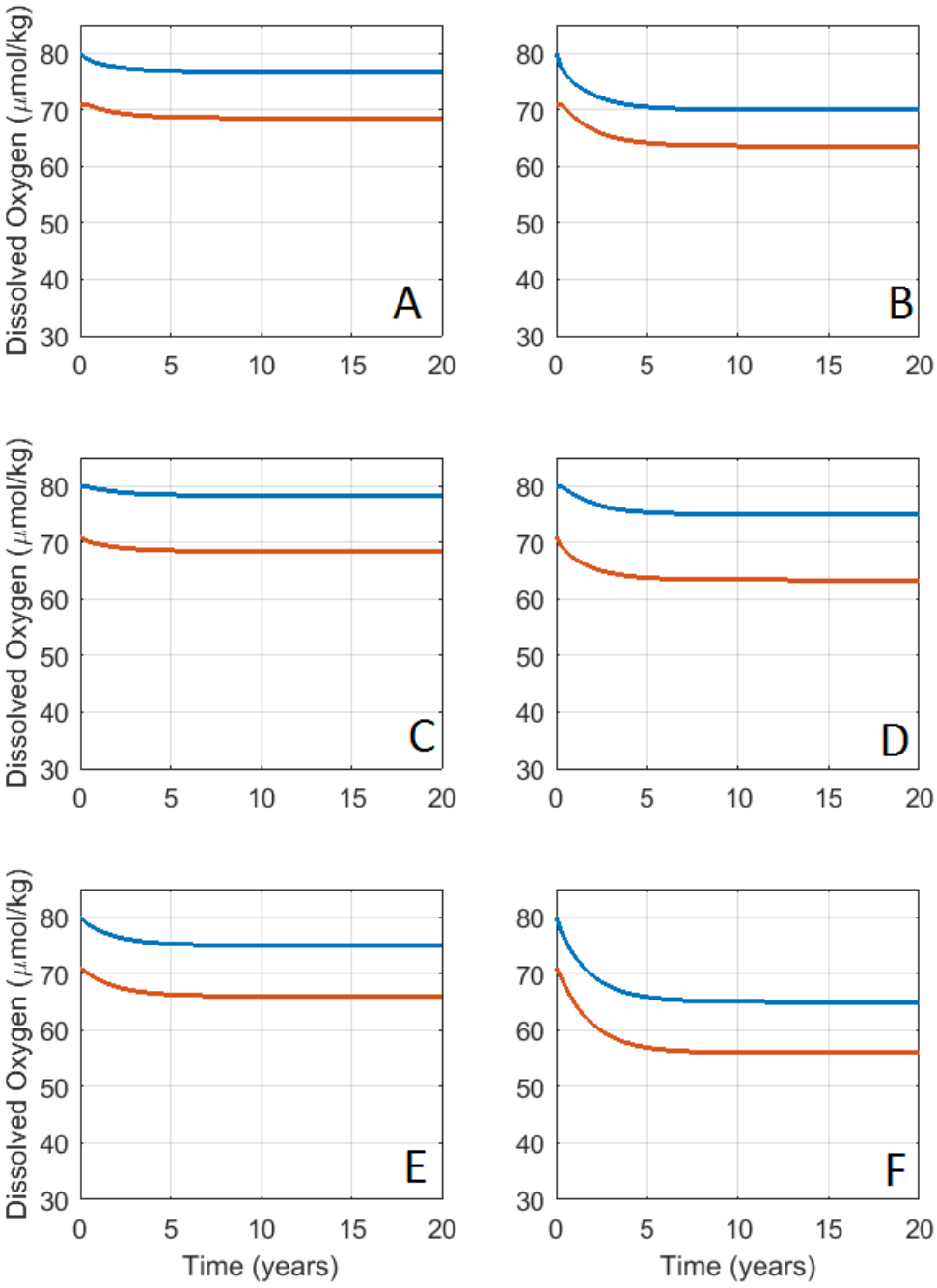

Figure 4.4. Box model runs with a step function perturbation in source waters. The inshore box concentration (orange) and the offshore box concentration (blue) are shown for a) a 5 μmol/kg change in the northern source water b) a 15 μmol/kg change in the northern source water c) a 5 μmol/kg change in the southern source water d) a 15 μmol/kg change in the southern source water e) a 5 μmol/kg change in both source waters and f) a 15 μmol/kg change in both source waters.

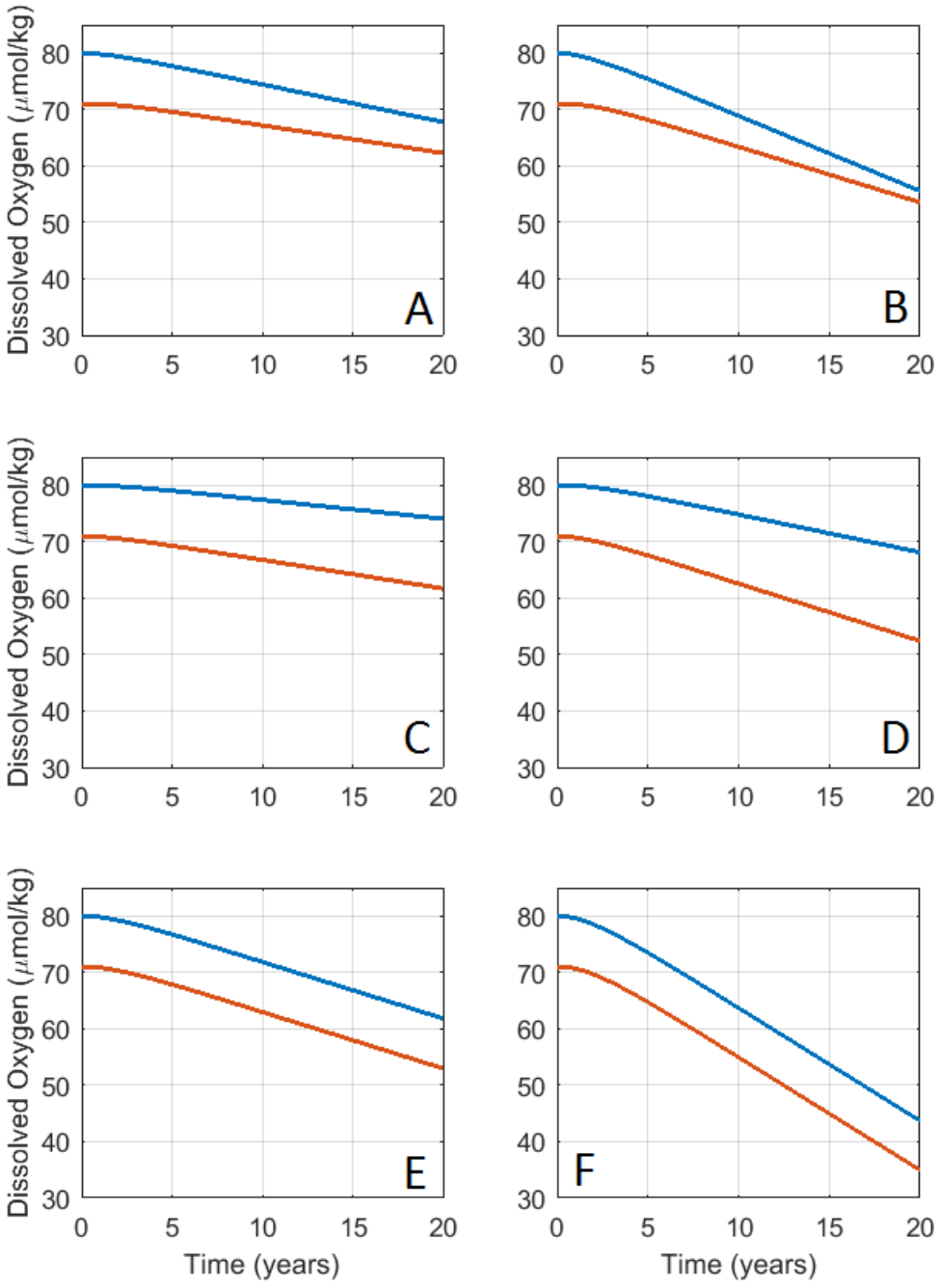

Figure 4.5. Box model runs with continuous decline in the source water dissolved oxygen concentration. The inshore box concentration (orange) and the offshore box concentration (blue) are shown for a) a 1 μmol/kg/year decline in the northern source water b) a 2 μmol/kg/year decline in the northern source water c) a 1 μmol/kg/year decline in the southern source water d) a 2 μmol/kg/year decline in the southern source water e) a 1 μmol/kg/year decline in both source waters and f) a 2 μmol/kg/year decline in both source waters.

The source water declines were also varied continuously. The scenario is comparable to the reports of oxygen decline in Southern California [*Bograd et al.*, 2008, 2015] which occured for over a 20-year period. While the report from Oregon is a comparison of two sets of data from two periods of time (the 1960s-1970s and the 2000s), it is assumed that the oxygen declined over a period of twenty or thirty years somewhat steadily as *Pierce et al.* [2012] report the decline using a linear regression model. The source waters were perturbed with an annual decline in oxygen of 1-2 μmol/kg (Figure 4.5).

The most realistic decline was again when both source waters were perturbed. When only one source water declined, there was a differential response of the oxygen concentrations in the inshore and offshore boxes. The offshore box declined faster than the inshore box when only the northern source water was perturbed and the inshore box declined faster when only the southern sourcewater was perturbed. Figure 4.6 tests the idea further by varying the southern source water by -3 μmol/kg/year. Though the inshore box declined around 30 μmol/kg, the offshore box declined around 17 μmol/kg which is a rate of less than 1 μmol/kg/year. When manipulating both source waters, the 2 μmol/kg perturbation more accurately achieved the 38 μmol decline over 20 years that approximates the observed declines.

The observed declines suggest that both the inshore and offshore regions declined at the same rate (Figure 3.7) on σ_θ 26.7. However, around σ_θ 26.5-26.7, the declines measured on station 80 are over 2.5 μmol/kg/year while the declines measured on station 65 are around 2 μmol/kg/year. The reported rates of oxygen decline from Oregon are also smaller than the reported rates of oxygen decline in Southern California, with the maximum reported decline around 1 μmol/kg/year in Oregon while around 2 μmol/kg/year in Southern California. For these reasons, we also tested a case with a 1 μmol/kg/year decline in the northern source water

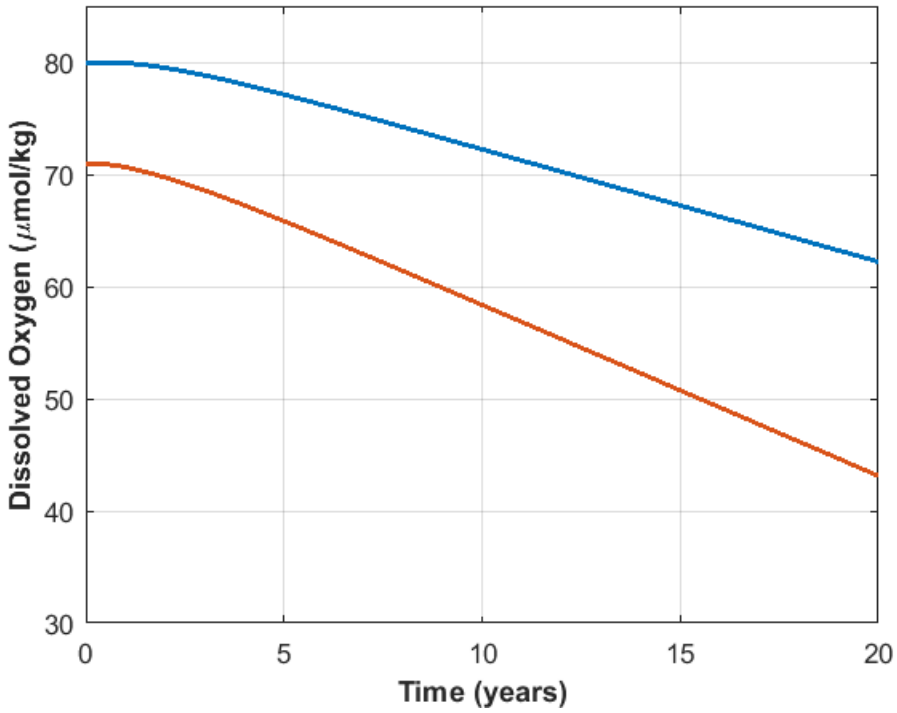

Figure 4.6. Box model run with a continuous decline in the southern source water of 3 μmol/kg/year. Shown are the inshore dissolved oxygen concentration (orange) and the offshore dissolved oxygen concentration (blue).

and a 2 μmol/kg/year decline in the southern source water (Figure 4.7). The decline in the offshore box was 24 μmol/kg while the decline in the inshore box was 27 μmol/kg. The result approached but was still not as large in magnitude as the observed declines.

4.3.2.2 Perturbations in the Alongshore Velocity

We tested a continuous perturbation in the alongshore velocity. In order to cause a decrease in the dissolved oxygen concentration in the inshore and offshore boxes, the mean flow of the offshore box should decrease or the mean flow of the inshore box should increase. The mean alongshore flow was halved for the offshore box only and the mean alongshore flow was doubled for the inshore box only (Figure 4.8). The response in terms of the oxygen concentrations in inshore and

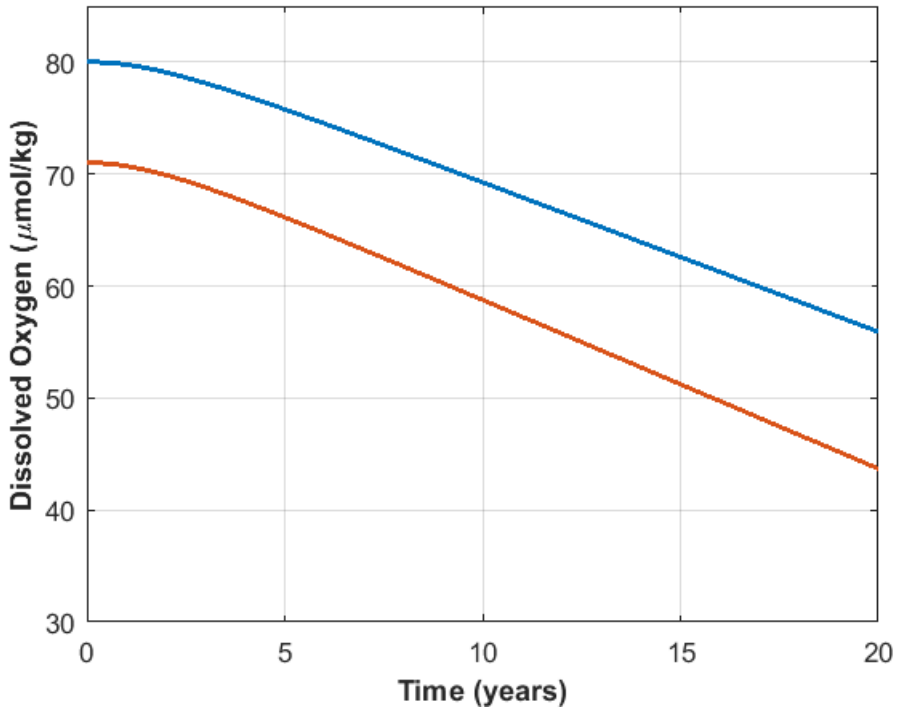

Figure 4.7. Box model run with a continuous decline in the northern source water of 1 μmol/kg/year and in the southern source water of 2 μmol/kg/year. Shown are the inshore dissolved oxygen concentration (orange) and the offshore dissolved oxygen concentration (blue).

offshore boxes was less than 10 μmol/kg. To attempt to achieve a larger change in oxygen concentration, the offshore mean flow was halved and the inshore mean flow was tripled to 3 cm/s (Figure 4.9). The response of the inshore box and offshore boxes was a decrease of 14 μmol/kg and roughly 15 μmol/kg respectively, over the 20-year simulation period. The decreases remain less than half of the declines expected from the observed rate of decline along Line 67.

The stepfunction perturbation in the alongshore velocity produced a decrease in dissolved oxygen in the boxes which leveled off to a new equilibrium concentration, similar to the stepfunction perturbation in the sourcewater concentration.

4.3.2.3 Perturbations in Respiration

To test for the possible role of changes in respiration, we also continually increased the respiration from the steady state value to a new value. The steady state respiration of the initial simulation model was 1.68 μmol/kg/year and was increased to a final respiration rate of 2.68 and 3.68 μmol/kg/year (Figure 4.10). The maximum change for the inshore and offshore boxes was a decrease of 13 and 14 μmol/kg over the time period respectively. From the Martin curve, the corresponding respiration profile suggests an exponential decrease in dissolved oxygen utilization from 20 μmol/L/year at 100 m to 5 μmol/L/year at 200 m and roughly 1 μmol/L/year at 500 m [*Martin et al.*, 1987]. An upper value for the new respiration rate around 4 μmol/kg/year is reasonable for 300 m depth in this region. Thus, a gradual increase over the 20 year time-period of 1 or 2 μmol/kg in respiration in the region alone is not driving the large declines in observed oxygen. Even considering changes in the depth at which respiration is occuring, the magnitude of the response (0.7 μmol/kg/year) is not strong enough to suggest that a change in the depth of respiration could fully explain the decreases in dissolved oxygen.

4.3.2.4 Changes in Cross-shore Mixing

We tested the effect of changing the mixing parameter, D, during the simulation 4.11. Increasing mixing over the time period deoxygenated the offshore box and oxygenated the inshore box. Decreasing mixing over the time period oxygenated the offshore box and deoyxgenated the inshore box. The oxygen concentrations in the observations decreased on both inshore and offshore stations. Thus, it is unlikely that a change in cross-shore mixing is driving dissolved oxygen declines on Line 67.

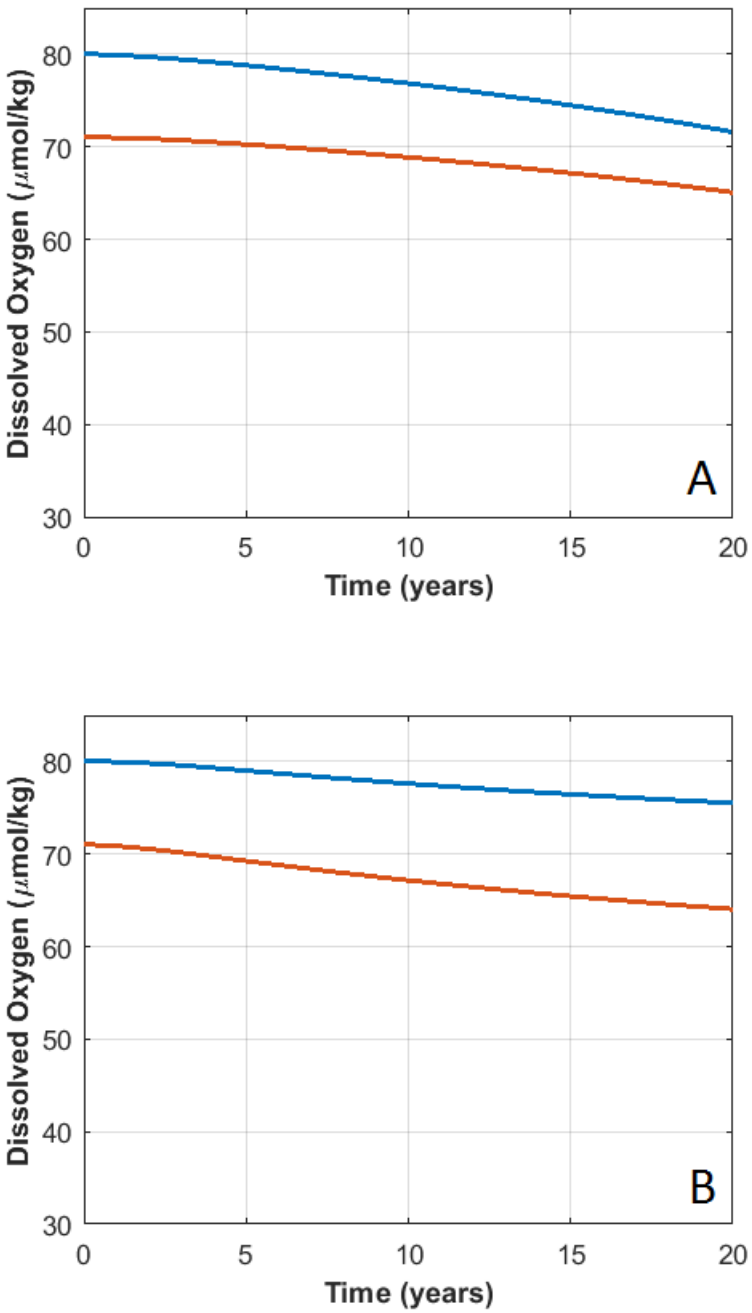

Figure 4.8. Box model runs with a) the offshore alongshore velocity halved to 0.5 cm/s and b) the inshore alongshore velocity doubled to 2 cm/s over the simulation period. Shown are the inshore dissolved oxygen concentration (orange) and the offshore dissolved oxygen concentration (blue).

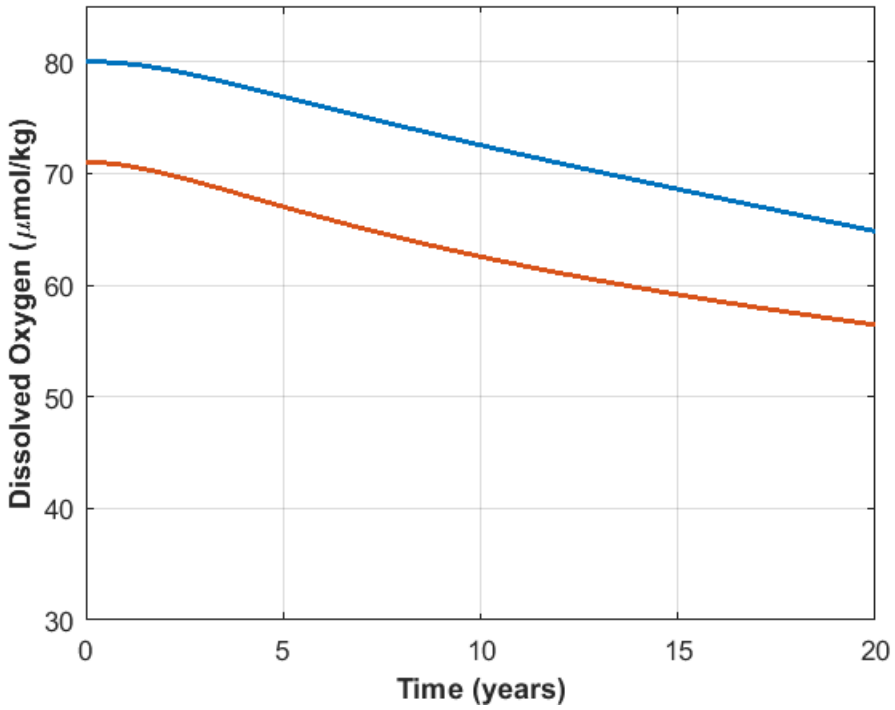

Figure 4.9. Box model run with the offshore alongshore velocity halved to 0.5 cm/s and the inshore alongshore velocity tripled to 3 cm/s. Shown are the inshore dissolved oxygen concentration (orange) and the offshore dissolved oxygen concentration (blue).

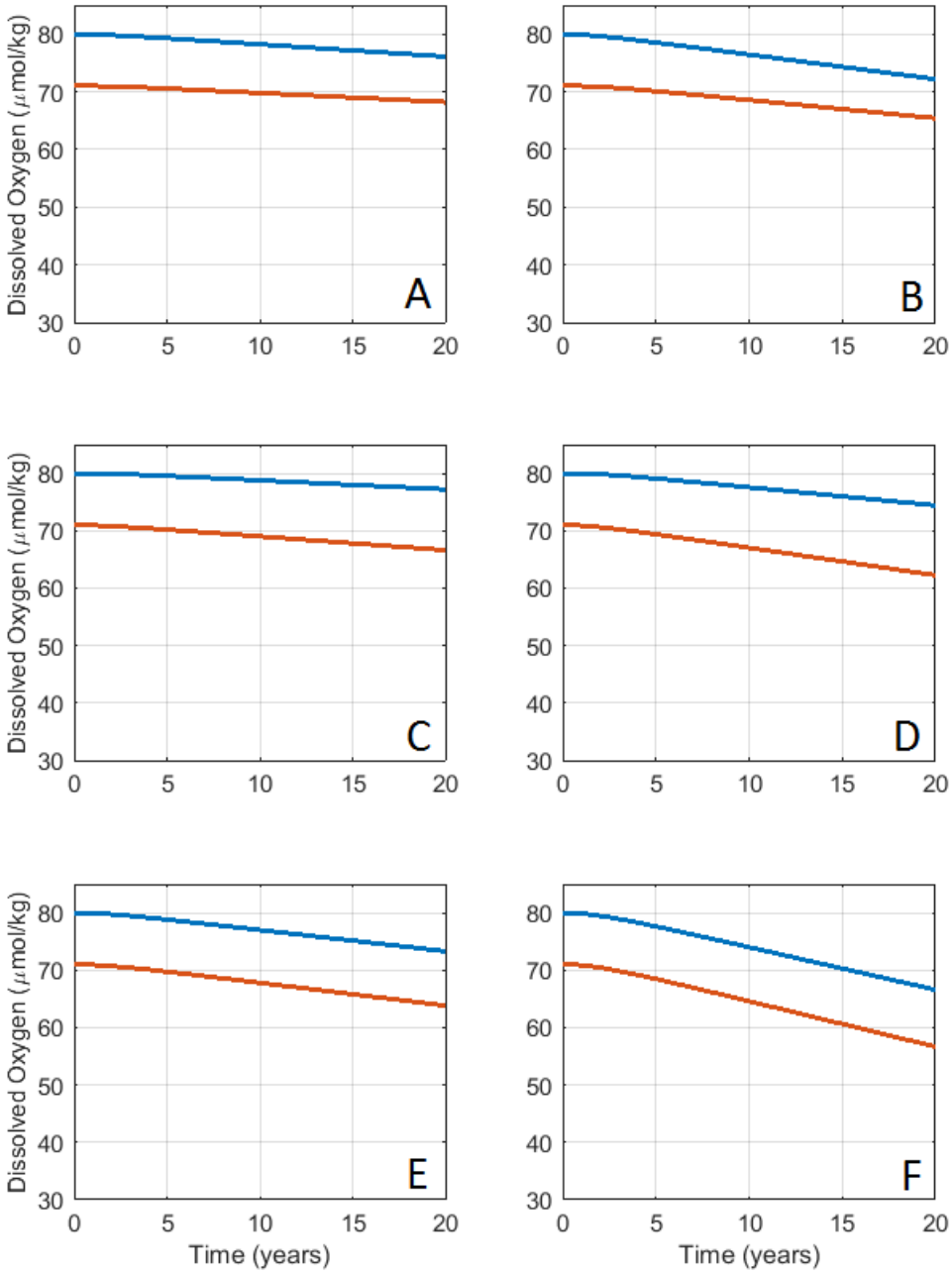

Figure 4.10. Box model runs with increases in local respiration. The respiration rate was gradually increased from 1.68-2.68 μmol/kg/year for a) the offshore box only c) the inshore box only and e) both inshore and offshore boxes, and from 1.68-3.68 μmol/kg/year for b) the offshore box only d) the inshore box only and f) both inshore and offshore boxes. Shown are the inshore dissolved oxygen concentration (orange) and the offshore dissolved oxygen concentration (blue).

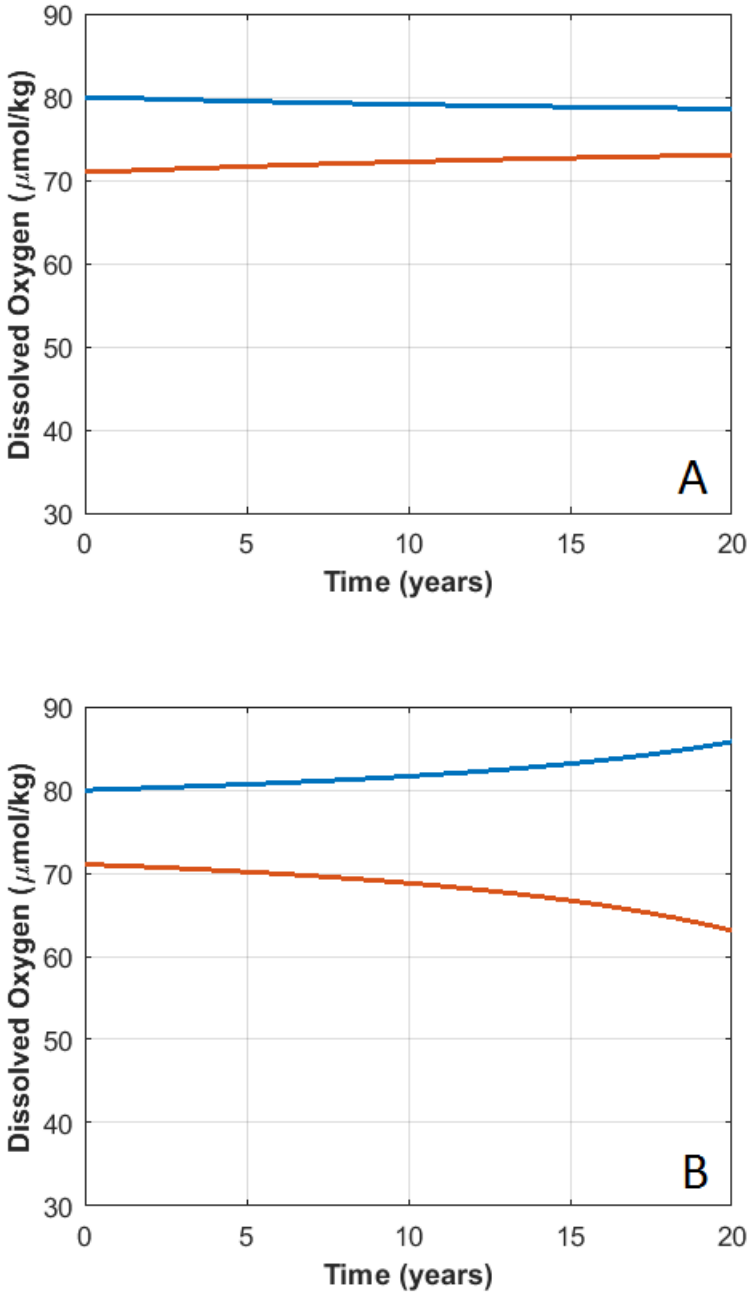

Figure 4.11. Box model runs with changes in the cross-shore mixing, D. The original D value is 209 m^2/s. D was increased by 8 m^2/s per year in (a) and decreased by 8 m^2/s per year in (b). Shown are the inshore dissolved oxygen concentration (orange) and the offshore dissolved oxygen concentration (blue).

4.3.2.5 Multiple Perturbations

Based on the reported observations in the literature, we could use a combination of forcings in the box model that is a reasonable representation of the observed forcings. For the source waters, the northern source water has decreased continuously by 1 μmol/kg/year while the southern source water has decreased continuously by 2 μmol/kg/year [*Bograd et al.*, 2008; *Pierce et al.*, 2012]. There is some indication of increasing surface chl-a concentration as measured from satellite in the Central California region. *Kahru et al.* [2009] found increases in net primary productivity and chl-a annual peak levels using satellite ocean color data from 1997 to 2007. In Central California, annual peak primary productivity calculated from satellite chl-a after 2003 was consistently above 2000 mg C/m^2/day while between 1998 and 2003 only two annual peaks reached 2000 mg C/m^2/day or higher. *Kahru et al.* [2012] merged additional satellite ocean color data to create a time-series from 1997-2012 and confirmed statistically significant chl-a increases in the coastal Central California region (defined in the manuscript as Area 3). In terms of the magnitude of the increase, *Thomas et al.* [2013] used a state space model to reveal a trend from 1998 to 2011 that suggest increases from 0.45 to 0.70 mg/chl-a/m^3 during the time period for roughly inshore of 300 km with increases 300-600 km from shore of 0.30 to 0.35 mg/chl-a/m^3. Removing the influence of the 1997/1998 El Nino, *Thomas et al.* [2013] found that the difference over the time period was weaker but still detected increases in chl-a in the area of Line 67 of 0.1-.25 mg/chl-a/m^3. Because the increase in chl-a was 22-56%, we take an estimate of the change in respiration in the box to be 50%, which is likely an upper estimate since a change in primary production at the surface translates to a less than proportional increase in carbon flux and the export ratio [*Pennington et al.*, 2010; *Pilskaln et al.*, 1996].

In terms of the alongshore mean flow and the mixing coefficient, D, there are no observed changes in these fields. These fields are very difficult to measure. In the geostrophic velocities calculated from the hydrographic profiles of temperature and salinity along Line 67, we found no statistically significant change in the mean alongshore current speeds. Further, an increase in the mixing coefficient oxygenates the inshore waters and deoxygenates the offshore waters, which is not found in the observations. Thus, in the cumulative forcing we did not include changes to the mean alongshore flow or the mixing coefficient, D.

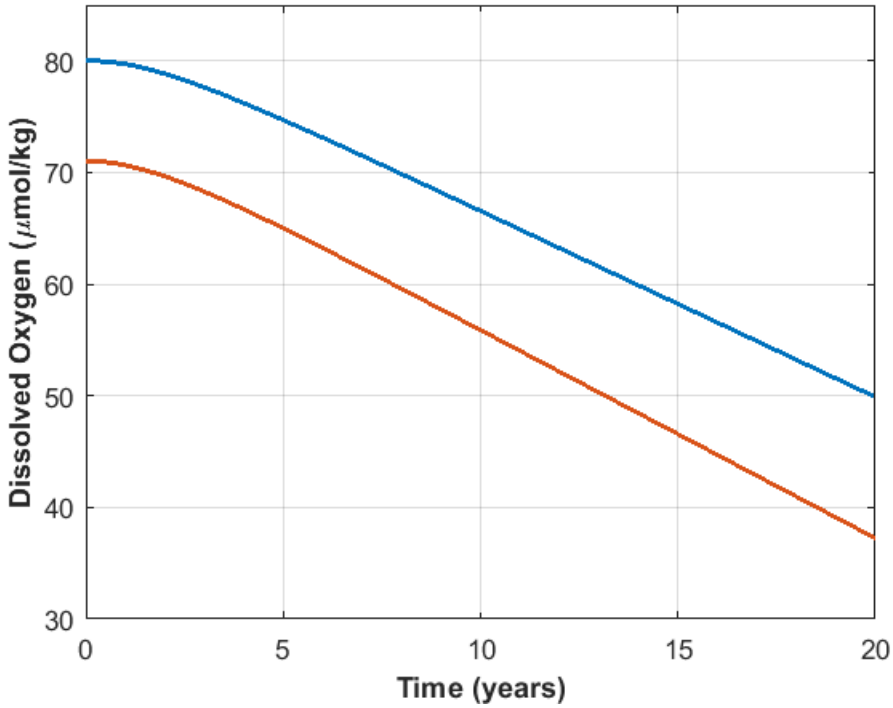

Figure 4.12. Box model run with source water declines and increased respiration. The northern source water dissolved oxygen declined at a rate of 1 μmol/kg/year, the southern source water dissolved oxygen declined at a rate of 2 μmol/kg/year, and respiration gradually increased from 1.68 μmol/kg/year to 2.52 μmol/kg/year. Shown are the inshore dissolved oxygen concentration (orange) and the offshore dissolved oxygen concentration (blue).

The cumulative forcing shows a reasonable reproduction of the observed declines in dissolved oxygen (Figure 4.12). The conclusion is that source water

changes from both northern and southern source waters are needed to reproduce the observed declines, as well as an extra source of decline such as from the local respiration.

While this conclusion is reasonable for looking from the vantage point of Line 67, there are additional implications. First of all, the declining source water concentrations from both the northern and southern regions suggest that large-scale oxygen loss processes from the North Pacific and the Equator are occuring. Second, since a stepfunction perturbation in the sourcewater concentration did not replicate the observed declines very well, it is likely that the oxygen loss processes are continuous and have been occuring for some time. In terms of ventilation, an isopycnal could be ventilated with increasingly lower frequency, or ventilation on the isopycnal could have stopped, which, with continued respiration, would imply a falling oxygen concentration. In terms of respiration, the imbalance between respiration and supply would have to be maintained over an extended time period and likely over a large spatial area. The interesting aspect of spatial extent is that it could imply a compounding effect; as a water parcel traveled, it would continue to add to its oxygen deficit. In the context of the box model, a source water decline of 2 μmol/kg/year could mean not only source water declines but also continued imbalance of respiration and supply on the journey to Line 67. The rates of source water decline chosen then, though they were on the high side of the reported observations, would appear to be more reasonable in terms of representing the dynamics of the system.

4.3.3 Sensitivity of the Model and Alternate Initial Conditions

The box model is a simple representation of the central California Current system. A few parameter sensitivities are of note, and they are the ratio of the volumes of the inshore and offshore boxes and the difference between the flux of

oxygen rich waters from the north and flux of oxygen deficient waters from the south.

The ratio of the volumes of inshore and offshore boxes were varied from the offshore box being 80% of the inshore box to being twice the inshore box volume. The range of values for the multiple perturbation case is shown in Figure 4.13. There was a 3-4 μmol/kg range in the dissolved oxygen concentration at the end of the 20-year simulation for different multiple perturbation runs.

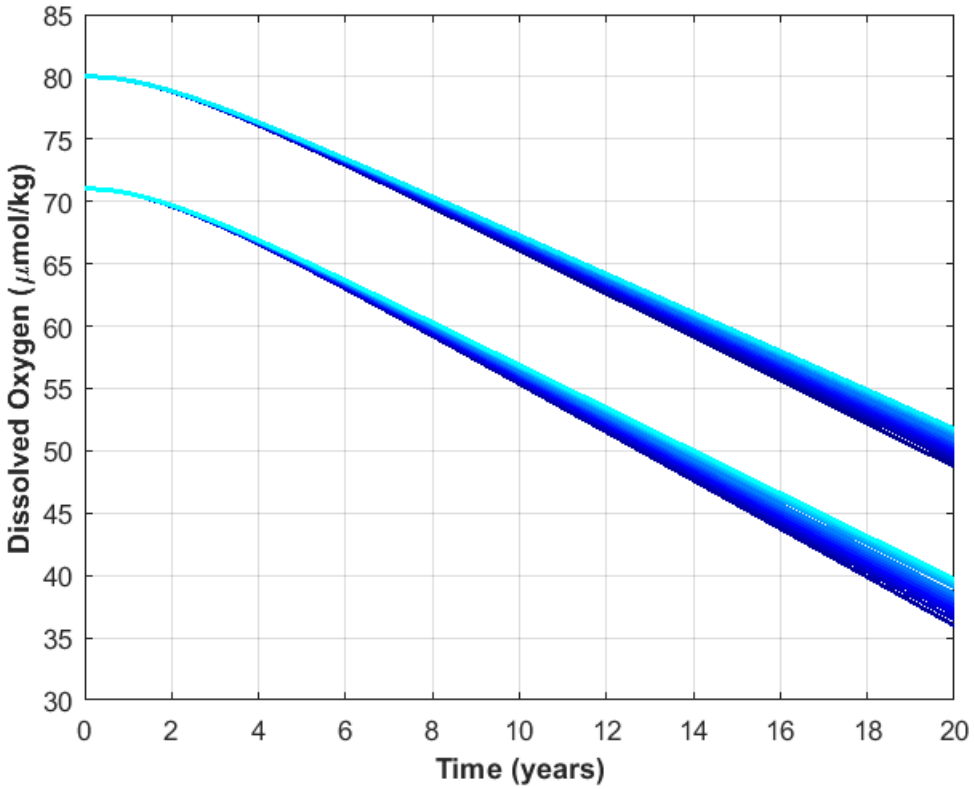

Figure 4.13. Model sensitivity runs of the multiple perturbation scenario changing the ratio of inshore and offshore box volumes. The offshore box volume was varied from 80% to 200% of the inshore box volume.

The difference between the offshore and inshore oxygen gradients were varied. The northern source water was decreased until the inflow of oxygen into the offshore box equaled the deficit in oxygen from the flow into the inshore box. The

northern source water was also increased by up to 5 μmol/kg. The multiple perturbation case was run from each of these new steady state cases (Figure 4.14). There is very little variation in the final dissolved oxygen concentration between the multiple perturbation runs.

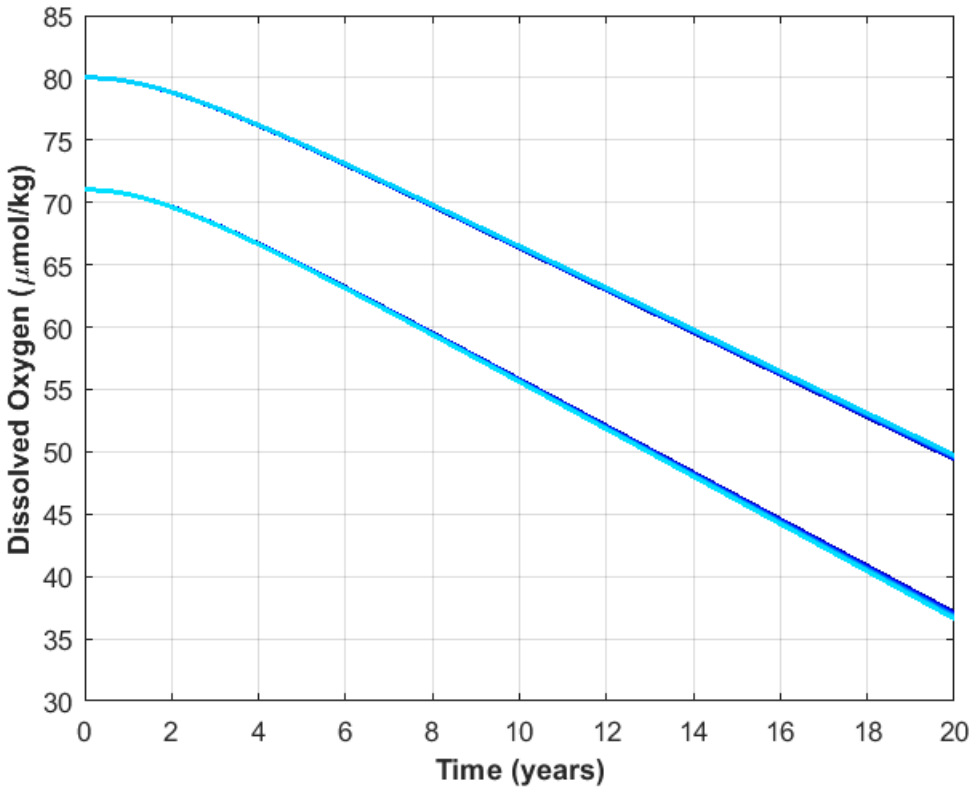

Figure 4.14. Model sensitivity runs of the multiple perturbation scenario changing the steady state northern source water concentration from 105-95 μmol/kg. The value used in standard runs was 100 μmol/kg.

Chapter 5
CONCLUSIONS

Observational evidence for declining dissolved oxygen concentrations at mid-depth in the Central California Current were presented. Hydrographic data along the CalCOFI transect Line 67 from 1998-2013 demonstrated that there was interannual variability in dissolved oxygen at the bottom of the mixed layer and a steep declining trend of 1.9 μmol/kg/year in dissolved oxygen along the density surface σ_θ 26.7. Over the 16-year period, the dissolved oxygen concentration declined nearly 40% in waters of σ_θ 26.7. The interannual variability is correlated with the spring upwelling index and suggests that short-term climatic factors have a large impact on dissolved oxygen concentrations in and near the mixed layer. A box model suggests that the declines along σ_θ 26.7, roughly at 300 m depth, are likely due to a combination of factors, which follows from the high rate of decline from 1998-2013. To explain the local declines, the box model points to oxygen declines in source waters from both north and south of the region, as well as an additional source which could be from increased respiration due to increased carbon flux from higher or more episodic primary production.

With regards to the three large thematic questions posed earlier, we are able to answer 1) and 2). Declining dissolved oxygen levels is a California Current-wide phenomenon, as the observational data presents. There may be region-specific ways in which the declines present themselves, perhaps exacerbated by shelf processes or modified by coastal circulation. However, the phenomenon of declining dissolved oxygen exists throughout the California Current system. The reason for the declines seems likely driven by source water dissolved oxygen concentration changes, with local respiration effects along Line 67 secondary but

also likely occuring. Thus, the primary reason for observed declines in Central California appears to be remote forcing. Further, we suggest that the remote forcing is occuring from at least two source water perturbations, one feeding the California Current and one feeding the California Undercurrent. We do not examine evidence as to the cause of the remote forcing; thus we do not attempt to answer the question of whether the observations are tied to decadal climate variability or climate change.

While we have presented data and analysis that moves thinking on the deoxygenation problem forward, there are still many questions left unanswered. Future work could investigate the environmental forcing of the region with a more complex model. In addition, wherever possible, time-series data measuring dissolved oxygen should be continued. In attacking the problem of climate change-induced deoxygenation, observations that track the ocean's response to climate change are essential. Further, existing time-series have the advantage of a history of data from which to draw conclusions.

Whether focused on observations of ocean deoxygenation or modeled impacts, it is clear that more study is required to understand ocean deoxygenation. Especially since model predictions suggest a less oxygenated ocean in the future, more regional and global studies are needed to elucidate explanations of present-day ocean deoxygenation and assess the validity of these future predictions.

REFERENCES

Bartlett, M. S., Some aspects of the time-correlation problem in regard to tests of significance, *Journal of the Royal Statistical Society*, *98*, 536–543, 1935.

Bograd, S. J., C. G. Castro, E. Di Lorenzo, D. M. Palacios, H. Bailey, W. Gilly, and F. P. Chavez, Oxygen declines and the shoaling of the hypoxic boundary in the california current, *Geophysical Research Letters*, *35*, 2008.

Bograd, S. J., M. P. Buil, E. Di Lorenzo, C. G. Castro, I. D. Schroeder, R. Goericke, C. R. Anderson, C. Benitez-Nelson, and F. A. Whitney, Changes in source waters to the southern california bight, *Deep Sea Research Part II: Topical Studies in Oceanography*, *112*, 42–52, 2015.

Chan, F., J. Barth, J. Lubchenco, A. Kirincich, H. Weeks, W. T. Peterson, and B. Menge, Emergence of anoxia in the california current large marine ecosystem, *Science*, *319*, 920–920, 2008.

Chelton, D. B., Large-scale response of the california current to forcing by the wind stress curl, *Calif. Coop. Oceanic Fish. Invest. Rep*, *23*, 130–148, 1982.

Chhak, K., and E. Di Lorenzo, Decadal variations in the california current upwelling cells, *Geophysical Research Letters*, *34*, 2007.

Cochrane, D., and G. H. Orcutt, Application of least squares regression to relationships containing auto- correlated error terms, *Journal of the American Statistical Association*, *44*, 32–61, 1949.

Collins, C. A., J. T. Pennington, C. G. Castro, T. A. Rago, and F. P. Chavez, The california current system off monterey, california: physical and biological coupling, *Deep Sea Research Part II: Topical Studies in Oceanography*, *50*, 2389–2404, 2003.

Collins, C. A., L. M. Ivanov, O. V. Melnichenko, and N. Garfield, California undercurrent variability and eddy transport estimated from rafos float observations, *Journal of Geophysical Research: Oceans*, *109*, 2004.

Collins, C. A., T. Margolina, T. A. Rago, and L. Ivanov, Looping rafos floats in the california current system, *Deep Sea Research Part II: Topical Studies in Oceanography*, *85*, 42–61, 2013.

Connolly, T. P., B. M. Hickey, S. L. Geier, and W. P. Cochlan, Processes influencing seasonal hypoxia in the northern california current system, *Journal of Geophysical Research: Oceans*, *115*, 2010.

Deutsch, C., H. Brix, T. Ito, H. Frenzel, and L. Thompson, Climate-forced variability of ocean hypoxia, *Science*, *333*, 336–339, 2011.

Deutsch, C., et al., Centennial changes in north pacific anoxia linked to tropical trade winds, *Science*, *345*, 665–668, 2014.

Di Lorenzo, E., et al., North pacific gyre oscillation links ocean climate and ecosystem change, *Geophysical Research Letters*, *35*, 2008.

Emerson, S., S. Mecking, and J. Abell, The biological pump in the subtropical north pacific ocean: Nutrient sources, redfield ratios, and recent changes, *Global Biogeochemical Cycles*, *15*, 535–554, 2001.

Emerson, S., Y. W. Watanabe, T. Ono, and S. Mecking, Temporal trends in apparent oxygen utilization in the upper pycnocline of the north pacific: 1980–2000, *Journal of Oceanography*, *60*, 139–147, 2004.

Garfield, N., C. A. Collins, R. G. Paquette, and E. Carter, Lagrangian exploration of the california undercurrent, 1992–95, *Journal of Physical Oceanography*, *29*, 560–583, 1999.

Garfield, N., M. E. Maltrud, C. A. Collins, T. A. Rago, and R. G. Paquette, Lagrangian flow in the california undercurrent, an observation and model comparison, *Journal of Marine Systems*, *29*, 201–220, 2001.

Grantham, B. A., F. Chan, K. J. Nielsen, D. S. Fox, J. A. Barth, A. Huyer, J. Lubchenco, and B. A. Menge, Upwelling-driven nearshore hypoxia signals ecosystem and oceanographic changes in the northeast pacific, *Nature*, *429*, 749–754, 2004.

Gruber, N., Warming up, turning sour, losing breath: ocean biogeochemistry under global change, *Philosophical Transactions of the Royal Society of London A: Mathematical, Physical and Engineering Sciences*, *369*, 1980–1996, 2011.

Hayward, T. L., and E. L. Venrick, Nearsurface pattern in the california current: coupling between physical and biological structure, *Deep Sea Research Part II: Topical Studies in Oceanography*, *45*, 1617–1638, 1998.

Huang, R. X., Heaving modes in the world oceans, *Climate Dynamics*, *45*, 3563–3591, 2015.

Kahru, M., R. Kudela, M. Manzano-Sarabia, and B. G. Mitchell, Trends in primary production in the california current detected with satellite data, *Journal of Geophysical Research: Oceans*, *114*, C02,004, 2009.

Kahru, M., R. M. Kudela, M. Manzano-Sarabia, and B. Greg Mitchell, Trends in the surface chlorophyll of the california current: Merging data from multiple ocean color satellites, *Deep Sea Research Part II: Topical Studies in Oceanography*, *77–80*, 89–98, 2012.

Keeling, R. F., and H. E. Garcia, The change in oceanic o2 inventory associated with recent global warming, *Proceedings of the National Academy of Sciences*, *99*, 7848–7853, 2002.

Keeling, R. F., A. Körtzinger, and N. Gruber, Ocean deoxygenation in a warming world, *Annual review of marine science*, *2*, 199–229, 2010.

Kwon, E. Y., C. Deutsch, S.-P. Xie, S. Schmidtko, and Y.-K. Cho, The north pacific oxygen uptake rates over the past half century, *Journal of Climate*, *29*, 61–76, 2016.

Martin, J. H., G. A. Knauer, D. M. Karl, and W. W. Broenkow, Vertex: carbon cycling in the northeast pacific, *Deep Sea Research Part A. Oceanographic Research Papers*, *34*, 267–285, 1987.

McClatchie, S., R. Goericke, R. Cosgrove, G. Auad, and R. Vetter, Oxygen in the southern california bight: Multidecadal trends and implications for demersal fisheries, *Geophysical Research Letters*, *37*, 2010.

Mecking, S., C. Langdon, R. A. Feely, C. L. Sabine, C. A. Deutsch, and D.-H. Min, Climate variability in the north pacific thermocline diagnosed from oxygen measurements: An update based on the u.s. clivar/co2 repeat hydrography cruises, *Global Biogeochemical Cycles*, *22*, n/a–n/a, 2008.

Meinvielle, M., and G. C. Johnson, Decadal water-property trends in the california undercurrent, with implications for ocean acidification, *Journal of Geophysical Research: Oceans*, *118*, 6687–6703, 2013.

Ono, T., T. Midorikawa, Y. W. Watanabe, K. Tadokoro, and T. Saino, Temporal increases of phosphate and apparent oxygen utilization in the subsurface waters of western subarctic pacific from 1968 to 1998, *Geophysical Research Letters*, *28*, 3285–3288, 2001.

Pennington, J. T., G. E. Friederich, C. G. Castro, C. A. Collins, W. W. Evans, and F. P. Chavez, *The Northern and Central California Coastal Upwelling System*, book section 2, pp. 29–44, Springer, Berlin, 2010.

Pierce, S. D., J. A. Barth, R. K. Shearman, and A. Y. Erofeev, Declining oxygen in the northeast pacific, *Journal of Physical Oceanography*, *42*, 495–501, 2012.

Pilskaln, C. H., J. B. Paduan, F. P. Chavez, R. Y. Anderson, and W. M. Berelson, Carbon export and regeneration in the coastal upwelling system of monterey bay, central california, *Journal of Marine Research*, *54*, 1149–1178, 1996.

Santer, B. D., T. M. L. Wigley, J. S. Boyle, D. J. Gaffen, J. J. Hnilo, D. Nychka, D. E. Parker, and K. E. Taylor, Statistical significance of trends and trend differences in layer-average atmospheric temperature time series, *Journal of Geophysical Research: Atmospheres*, *105*, 7337–7356, 2000.

Stramma, L., G. C. Johnson, J. Sprintall, and V. Mohrholz, Expanding oxygen-minimum zones in the tropical oceans, *Science*, *320*, 655–658, 2008.

Sydeman, W. J., S. A. Thompson, M. García-Reyes, M. Kahru, W. T. Peterson, and J. L. Largier, Multivariate ocean-climate indicators (moci) for the central california current: Environmental change, 1990–2010, *Progress in Oceanography*, *120*, 352–369, 2014.

Thomas, A. C., R. Mendelssohn, and R. Weatherbee, Background trends in california current surface chlorophyll concentrations: A state-space view, *Journal of Geophysical Research: Oceans*, *118*, 5296–5311, 2013.

Watanabe, Y. W., T. Ono, A. Shimamoto, T. Sugimoto, M. Wakita, and S. Watanabe, Probability of a reduction in the formation rate of the subsurface water in the north pacific during the 1980s and 1990s, *Geophysical Research Letters*, *28*, 3289–3292, 2001.

Whitney, F. A., H. J. Freeland, and M. Robert, Persistently declining oxygen levels in the interior waters of the eastern subarctic pacific, *Progress in Oceanography*, *75*, 179–199, 2007.

Wunsch, C., The interpretation of short climate records, with comments on the north atlantic and southern oscillations, *Bulletin of the American Meteorological Society*, *80*, 245–255, 1999.

Wyrtki, K., The oxygen minima in relation to ocean circulation, *Deep Sea Research and Oceanographic Abstracts*, *9*, 11–23, 1962.

BIOGRAPHY OF THE AUTHOR

Alice Sonya Ren was born in Worcester, Massachusetts. She attended Carolyn T. Douglas elementary school in Acton, Massachusetts, R. J. Grey Jr. High School in Acton, Massachusetts, and Acton-Boxborough Regional High School in Acton, Massachusetts from which she graduated in 2007. She attended college at Duke University in Durham, NC where she earned a Bachelor of Science degree in Environmental Science in Fall 2010. She has completed internships at the National Oceanic and Atmospheric Administration (NOAA) and the Monterey Bay Aquarium Research Institute (MBARI). She began the graduate program in Oceanography at the University of Maine in Fall 2013. Alice S. Ren is a candidate for the Master of Science degree in Oceanography from The University of Maine in December 2016.